Nat. Hazards Earth Syst. Sci., 26, 4153–4175, 2026
https://doi.org/10.5194/nhess-26-4153-2026

Natural Hazards and Earth System Sciences
Open Access
EGU

Unveiling the link between extreme precipitation events and flood disasters in China: from a 3D perspective

Jie Wang[1,2,3], Sixuan Li[4], Xiaodan Guan[1,4], Ashok Kumar Pokharel[1], Yongli He[1,4], Chenyu Cao[4,5], Lulu Lian[1,4], and Lihui Zhang[1,4]

[1]Collaborative Innovation Center for Western Ecological Safety, Lanzhou University, Lanzhou, China
[2]Key Laboratory of Urban Meteorology, China Meteorological Administration, Beijing, China
[3]China Meteorological Administration Hydro-Meteorology Key Laboratory, Beijing, China
[4]School of Atmospheric Sciences, Lanzhou University, Lanzhou, China
[5]College of Earth and Environmental Sciences, Lanzhou University, Lanzhou, China

Correspondence: Jie Wang (wang_jie@lzu.edu.cn) and Xiaodan Guan (guanxd@lzu.edu.cn)

Received: 25 September 2025 – Discussion started: 10 November 2025
Revised: 22 May 2026 – Accepted: 12 August 2026 – Published: 27 August 2026

Abstract. Extreme precipitation events and their triggered flood disasters have received increasing attention owing to their severe threats to human lives and socioeconomic development. However, there is still a lack of research on their evolutionary characteristics and driving factors from a three-dimensional (3D) event-based perspective. Here, we developed a 3D automatic recognition algorithm based on the 3D connected component algorithm. This method was applied to investigate the 3D characteristics (i.e., accumulated magnitude, accumulated affected area, centroid, lifespan, moving direction, and moving distance) of 632 flood-causing precipitation (FCP) events in China from 2000 to 2023. The associated flood disasters and their underlying driving factors were further analysed. The 3D characteristics of FCP events show insignificant increasing trends in China during 2000–2023. The FCP events with larger accumulated magnitudes and affected areas are mainly distributed in the central Southern China (SC) and Northern China (NC), mostly moving eastward with longer distances and lifespans. Correspondingly, the flood characteristics (i.e., surface runoff and river discharge) of these FCP events also exhibit increasing trends, with high-magnitude surface runoff and river discharge events concentrated mainly in the central SC and NC. FCP-induced flood disasters are more severe in SC and parts of NC, while a relatively high proportion of flood disaster losses are concentrated in the southeastern fringe of the Qinghai-Tibetan Plateau (TP) and southwestern China (SWC). Notably, despite the increase in 3D characteristics of FCP events over the past two decades, flood disasters have shown a significant reduction, except for the direct economic losses. Driving factor analysis indicates that the combination of precipitation and environmental factors has the greatest explanatory power for flood disasters in the most regions of China, while human activities have a prominent impact on the flood disasters in the center of SC and NC. These findings provide new insights into the characteristics of FCP events and their associated flood disasters from a 3D event-based perspective.

1 Introduction

Flooding induced by extreme rainfall is one of the most hazardous natural disasters, posing significant threats to human security and socioeconomic development worldwide (Jevrejeva et al., 2018; Rentschler et al., 2022). Over the past decade, under the context of global warming and an intensifying hydrological cycle, the frequency and magnitude of destructive floods have been escalated due to the increased frequency of extreme precipitation (Blöschl et al., 2019; Wasko et al., 2021), resulting in immense economic devastation and loss of human lives (Rentschler et al., 2022; Islam and Wang, 2024). According to the Emergency Events Database (EM-DAT) of the Centre for Research on the Epidemiology of Disasters (CRED), a total of 4845 flood disasters occurred from 1980 to 2020, causing average annual economic losses exceeding USD 21 billion and approximately 5900 deaths per year. Therefore, rainstorm-induced flood disasters have become a crucial issue restricting the sustainable and healthy development of the global economy and society.

Heavy precipitation is a prominent factor leading to floods, and its amount, intensity, and duration determine the flooding process in regions where rainfall plays the dominant role in flood occurrence (Mallakpour and Villarini, 2015; Do et al., 2020b). Extensive research has examined the changes of extreme precipitation at regional and global scales using a range of indices and detection methodologies (Westra et al., 2013; Asadieh and Krakauer, 2015; Ban et al., 2015; Wu et al., 2019; Chinita et al., 2021). These studies reported that the frequency and intensity of heavy precipitation have increased. Some research using rain gauge observations suggested that sub-daily heavy precipitation may have increased more than daily heavy precipitation (Chinita et al., 2021). The concerns about such super-adiabatic increase have further been raised by modeling simulation, which projected further to increase between 2 % and 10 % by 2100 under a high-emissions scenario (Kharin et al., 2013). Notably, the heaviest and rarest precipitation events were projected to have the largest increase in frequency and intensity (Thackeray et al., 2022). The dominant driving factor of increment of extreme precipitation is the thermodynamic increase due to a 6–7 % $^{\circ}C^{-1}$ increase in the saturation vapor pressure of the atmosphere, which was dictated by the Clausius-Clapeyron (CC) relationship (Trenberth et al., 2003). Hiraga et al. (2025) suggested that probable maximum precipitation magnitude events become more frequent with annual exceedance probability increasing by about 10^1–10^2 from the historical to +4 K climatic conditions. Meanwhile, moisture and buoyancy increase associated with temperatures increase can trigger extreme precipitation intensification exceeding the CC scaling rate (i.e., super-CC scaling) (Fowler et al., 2021). In addition, dynamical drivers linked to shifts in global circulation modify extreme rainfall occurrence by altering the storm tracks and propagation speeds (Chan et al., 2023; Wasko et al., 2024). However, despite the observed and projected increase in extreme precipitation, the flood magnitude and frequency exhibit mixed trend patterns. Several global scale flood trend detection studies have found that more stations exhibit significant decreasing trends in flood magnitude than increasing ones (Do et al., 2017; Hodgkins et al., 2017; Wasko et al., 2021). These inconsistencies highlight the nonlinear relationship between precipitation intensity and flood disasters, driven by multiple interacting factors such as land use, hydrological capacity, and human interventions (Sharma et al., 2018; Do et al., 2020a). Therefore, understanding of how changes in extreme precipitation convert into flood impacts remains a critical research challenge.

Several previous studies have attempted to quantify the relationship between heavy precipitation and flood damage using statistical analysis and hydrological model simulations (Kundzewicz et al., 2014; Wei et al., 2018; Davenport et al., 2021; Rashid et al., 2023; Teale and Winter, 2024). For instance, Kundzewicz et al. (2014) reviewed evidence showing that changes in precipitation contribute to increased flood damages. Similarly, Davenport et al. (2021) estimated that increasing heavy precipitation contributed approximately 36 % of cumulative flood damages from 1988 to 2017 in the U.S. Looking forward, Rashid et al. (2023) developed a probabilistic model based on the probability of property damage and heavy precipitation indicators, indicating an increase in high property damage in the future. However, an extreme precipitation event often propagates in both space and time during flooding periods (Wang et al., 2025). Most previous studies have focused on isolated extreme precipitation properties (e.g., magnitude and intensity) without considering the impact of comprehensive spatiotemporal evolution characteristics of precipitation systems (e.g., moving direction, distance, and lifespan), which can critically influence flood damages (Wei et al., 2018; Davenport et al., 2021; Rashid et al., 2023). This gap limits our ability to quantify the impact of heavy precipitation characteristics on flood damages within individual precipitation events.

China has been the country most affected by hydrological and meteorological disasters, suffering from significant economic losses and numerous fatalities over the past several decades (Wei et al., 2018). Many studies examined the spatial-temporal characteristics of flood damages and evaluated the relationships between rainfall and flood damages, but few have investigated these characteristics from an event-based evaluation perspective (Li et al., 2012; Chen et al., 2021; Jia et al., 2022; Wang et al., 2022). Thus, more systematic, and reasonable studies are urgently needed in this aspect. Here, we perform the first study to improve our understanding of how changes in the evolutionary characteristics of heavy precipitation impact flood damages at an event perspective using a large precipitation sample (1042) and the flood damage metrics including destroyed cropland area, direct economic loss, affected population, and death population during rainfall period from 2000 to 2023 across China. In doing so, we used three-dimensional (3D) connected component algorithm, which is similar to that of Wang et al. (2025), to explore the evaluation characteristics of flood-causing rainstorm events in China. The flood characteristics and damages caused by each rainstorm were analysed for individual precipitation events. Finally, the underlying driving factors of flood disasters were assessed from an event-based perspective. This study will provide a deeper understanding of historical flood risk trends and enable accurate prediction of fatalities and losses based on the precipitation characteristics.

2 Data

2.1 River discharge from the Global Flood Awareness System

The Global Flood Awareness System (GloFAS, http://www.globalfloods.eu/, last access: 19 August 2026) couples the surface and sub-surface runoff from the Hydrology Tiles ECMWF Scheme for Surface Exchanges over Land (HTESSEL) land surface model, driven by the ECMWF's latest global atmospheric reanalysis (ERA5), with the LISFLOOD hydrological and channel routing model (Harrigan et al., 2020). The GloFAS-ERA5 river discharge reanalysis product is a global gridded available from 1979 to the present at a spatial resolution of 0.1° and a daily time step. The dataset is openly available through the Copernicus Climate Change Service (C3S) Climate Data Store (CDS) at https://ewds.climate.copernicus.eu/datasets/cems-glofas-historical?tab=download (last access: 10 May 2026). Harrigan et al. (2020) assessed the hydrological performance of GloFAS-ERA5 against observations from global in-situ river discharge stations; they used modified Kling–Gupta Efficiency Skill Score (KGESS), and found that the GloFAS-ERA5 reanalysis product is skilful in 86 % of catchments. Thus, the long temporal coverage, global consistency, and reliable simulation skill make GloFAS-ERA5 a valuable dataset for identifying extreme hydrological events such as floods. In this study, we collect GloFAS-ERA5 daily river discharge data of the rainy seasons (i.e., May–October) during 2000–2023.

2.2 ERA5 reanalysis precipitation and surface runoff data

The GloFAS-ERA5 river discharge reanalysis is produced by coupling the land surface model runoff component of the ECMWF ERA5 global reanalysis with the LISFLOOD hydrological and channel routing model (Harrigan et al., 2020). The LISFLOOD model is forced with daily HTESSEL surface and subsurface runoff from ERA5. In order to be consistent with the GloFAS-ERA5 river discharge, the precipitation and surface runoff fields from ERA5 were selected to analyse the spatiotemporal evolution patterns of rainstorm events and runoff generation processes over mainland China with high spatial (0.25°) and temporal (1 h) resolution covering the period 2000 to 2023. As one of the latest high-resolution climate reanalysis datasets, ERA5 is a global atmospheric reanalysis product developed by ECMWF using the 4D-Var data assimilation technique (Hersbach et al., 2020). Compared with other reanalysis datasets, such as MERRA-2, NCEP/NCAR, and JRA55, the ERA5 performs better for precipitation and extreme precipitation over China, although its performance is not as good as that of satellite-based data (e.g., the Integrated Multi-satellite Retrievals for Global Precipitation Measurement (GPM) (IMERG) precipitation product) (Jiang et al., 2023). Note that the ERA5 underestimates the frequency of occurrence and interannual variability of mesoscale convective systems (MCSs) (Alpizar et al., 2026). The ERA5 reanalysis precipitation product used in this study is accessible in C3S Climate Data Store (https://cds.climate.copernicus.eu/datasets, last access: 10 May 2026).

2.3 Flood disaster data

Historical flood damages data in 31 provincial administrative regions in China from 2000 to 2023 were obtained from the Meteorological Disaster Yearbook (MDY) in China. The data primarily include the flood records (i.e., flood location, affected area, and date of the event) as well as corresponding direct economic losses, the number of people affected, the number of deaths, and the affected cropland area. The MDY of China is currently the most comprehensive freely available source for accessing the flood records in China, and has been widely used in previous studies (Li et al., 2012; Wei et al., 2018; Shi et al., 2020; Wang et al., 2025). Unfortunately, this dataset has not been updated since 2020, thus, we supplemented flood disaster data from 2020 to 2023 using news reports and government sources by searching for the keywords “flood” and “inundation” online. All supplemented flood disaster data are derived from official released records, which guarantees their authenticity. Notably, although rainstorm flood records were collected from multiple sources, they represented authentic and valid disaster records and could accurately reflect the impacts caused by flood disasters.

A total of 1041 flood disaster records were obtained from MDY. The spatial-temporal distribution of these flood occurrence records across mainland China from 2000 to 2023 is depicted in Fig. 1. The accumulated flood occurrences frequency generally shows a decreasing trend from southeast to northwest (Fig. 1a), which is consistent with the distribution pattern of annual precipitation in China (Ma et al., 2015). The temporal variation of flood records in Fig. 1b shows that more flood disasters occurred during 2002–2010.

2.4 Flood disaster influencing factors

Meteorological, environmental, and anthropogenic factors are the primary drivers of flood occurrence in any region. Among meteorological conditions, rainfall is typically the primary cause of flood disasters. In this study, the 3D precipitation features (including accumulated area, accumulated magnitude, lifespan, and moving distance; presented in detail in Sect. 3.3) are selected to determine their influence on the spatial distribution of flood disasters. The environmental factors are important components of the disaster-forming environment (Ke et al., 2025). We selected cropland, normalized difference vegetation index (NDVI), slope, and elevation difference to represent cropland area, vegetation coverage, gradient of the land surface, and elevation

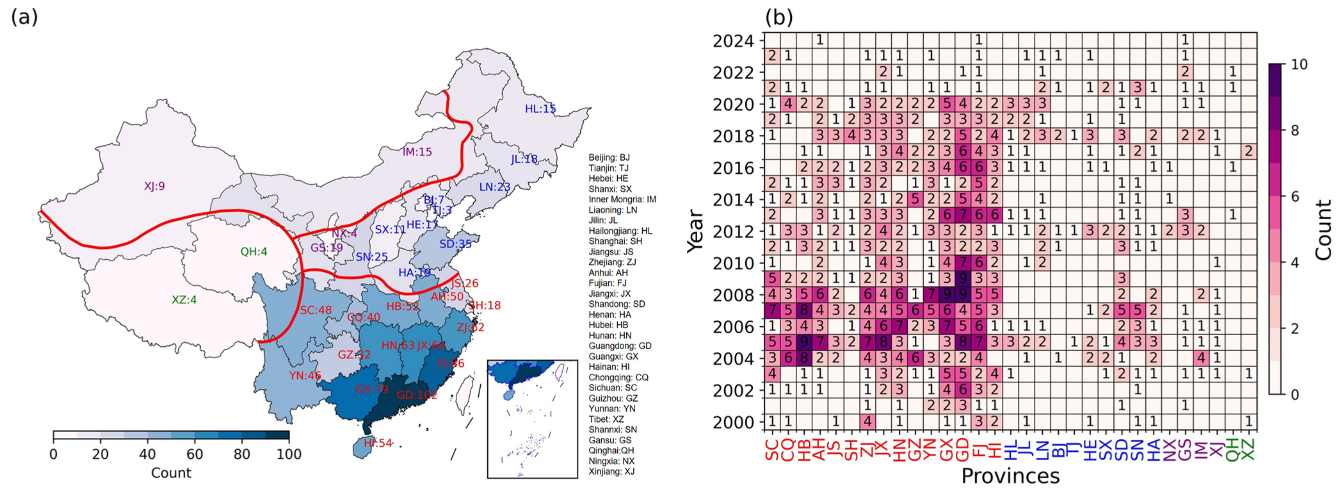

Figure 1. (a) Spatial distribution of accumulated flood records in China during 2020–2023. **(b)** Heat map of temporal variation of flood records for each province in China during 2020–2023. The characters in Fig. 1a denote the abbreviations of Chinese provincial names. The red lines indicate the division of four subregions: Northwestern China (NWC, purple font), Northern China (NC, blue font), Southern China (SC, red font), and Qinghai-Tibetan Plateau (TP, green font).

Table 1. Data of environmental and human activity factors.

Variable Name	Source	Accuracy	Time	Description
Cropland	https://doi.org/10.5281/zenodo.7936885 (Tu et al., 2023)	30 m × 30 m	2020	Cropland area, km^2
NDVI	RESDC	1 km × 1 km	2020	Average NDVI
Slope	RESDC	90 m × 90 m	2003	Average slope, °
Elevation differences	RESDC	90 m × 90 m	2003	Average elevation differences, m
Population	RESDC	1 km × 1 km	2000/2005/2010/2015/2020	Population density, person per km^2
GDP	RESDC	1 km × 1 km	2000/2005/2010/2015/2020	Economic density, CNY 10 000 km^{-2}

variations, as the environmental factors in this study. Additionally, human activity substantially modifies the natural environment and influencing flood disasters (Guan et al., 2021). Based on the existing research (Wu et al., 2021; Hoang and Liou, 2024), the population density and gross domestic product (GDP) were selected as important indicators to reflect human activity. All environmental and human activity factors were obtained from the Resource and Environment Data Cloud Platform (http://www.resdc.cn, last access: 19 August 2026), except for cropland, which was sourced from https://doi.org/10.5281/zenodo.7936885 (Tu et al., 2023, 2024). The original data were interpolated with the same spatial resolution of the precipitation with 8 km. In addition, it is worth noting that the population and GDP data were summed within grids cells. However, due to the lack of annual dataset, population and GDP data from 2000–2024 at 5-year intervals are included here. A summary of all variables and their data sources is presented in Table 1.

3 Methodology

3.1 Definition of precipitation threshold values

Following the definition of short-duration heavy rainfall events by the China Meteorological Administration (CMA), an hourly rainfall amount exceeding 16 mm is commonly defined as a heavy rainfall event, which has been validated by Zhang and Zhai (2011) to be a reasonable criterion to study short-duration heavy rainfall events in China. However, the significant spatial-temporal variations may occur in extreme events as a result of varying geographical and meteorological conditions and consequently, the threshold of extreme precipitation events varies across regions. For instance, hourly extreme precipitation exceeding 16 mm h^{-1} is relatively more frequent over the southern China, but it would be rather rare in the northwestern China (Fig. 2b). Thus, a fixed threshold cannot be used to extract relatively independent extreme precipitation events over China. In previous studies,

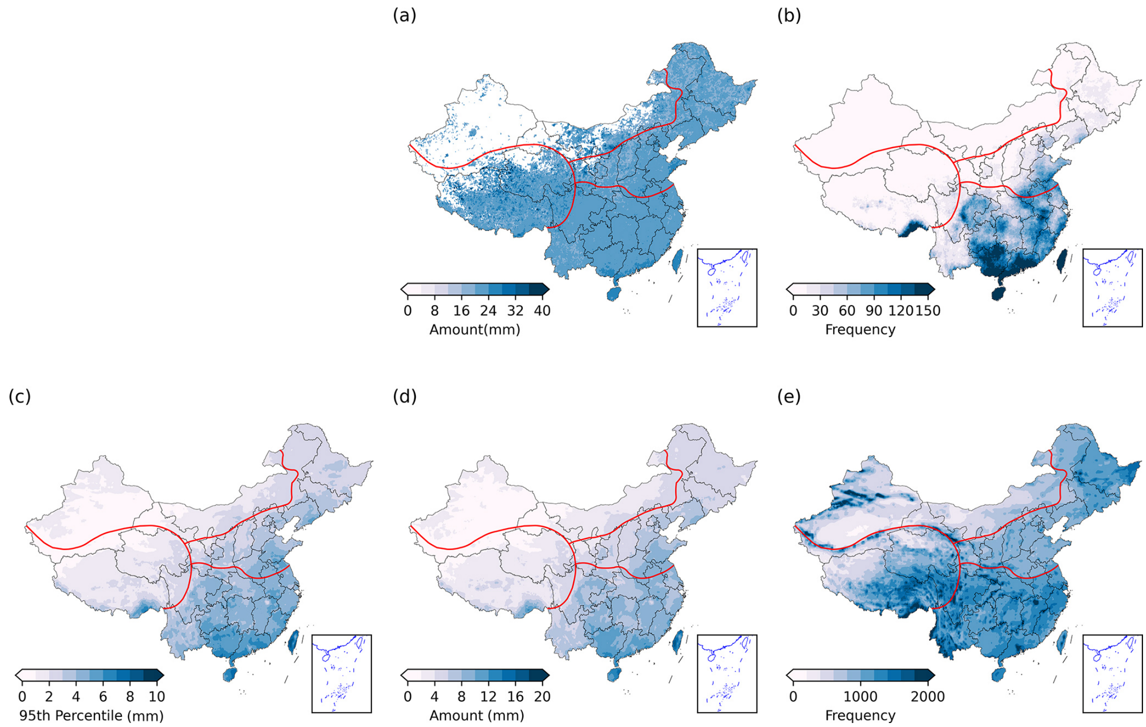

Figure 2. Spatial distributions of extreme precipitation amount **(a, d)** and frequency **(b, e)** calculated using the single threshold (> 16 mm) in first row and 95 % percentile (Fig. 2c) in second row, respectively. **(c)** Spatial distribution of 95 percentile of precipitation sequence during 2000–2024.

most existing studies defined the extreme precipitation events using the 90 % or 95 % percentile of the ordered precipitation sequence during the study period because of its simplicity (Gu et al., 2022). In this study, the 95 % percentile of precipitation sequence at each grid was defined as the thresholds for extreme events (Fig. 2c). Hourly precipitation amounts exceeding the extreme precipitation threshold were classified as extreme precipitation events. Figure 2d and e illustrate the spatial distribution of the amount and accumulated frequency of extreme precipitation, respectively. Overall, extreme precipitation is observed across China, with higher frequency is in the southeast than in the northwest. Subsequently, these threshold values were further applied to better extract the characteristics of contiguous extreme precipitation events.

3.2 Identification of flood-causing precipitation events

Historical flood damage sample datasets record flood events at country level in each province and provide the location and date of each flood event from 2000 to 2023. However, a single flood-causing precipitation (FCP, it is an extreme precipitation event that triggers flood disasters at the regional scale.) event mostly occurs synchronously across neighbouring regions or consecutively on adjacent days, leading to multiple flood records generated by one continuous precipitation process. In this study, we propose a precipitation event identification algorithm to identify relatively independent extreme precipitation events corresponding to each recorded flood disaster. The main steps of the precipitation event identification algorithm are described as follows (Fig. 3):

1. Determining the start and end times of flood-causing precipitation event: For each flood event (E_i), the approximate occurrence time (t_i) is obtained from the flood disasters dataset. Based on the previous studies, the lifespan of an FCP event is generally no longer than 3 d, and it is rare for such events to last more than 7 d (Wang et al., 2022). Thus, in order to detect all potentially associated persistent FCP events, we extract the FCP identification period for the 5 d before and after t_i. Subsequently, we use the vector shapefile of the flood-affected areas (l_i) as a spatial mask to isolate ERA5 precipitation within the affected area during identification period. Based on the precipitation time-series, we can accurately determine the start and end time of FCP event.

2. Determining the FCP event in flood-affected area: The accumulated precipitation during the start and end times of the FCP event (E_i) is first marked when its accumulated amount (P) exceeds the threshold value. The threshold value is the mean of 95 percentile of hourly precipitation amounts within the flood-affected area. The 95 % percentile value is computed from all rainy hours ($P > 0.1$ mm) during the rainy sea-

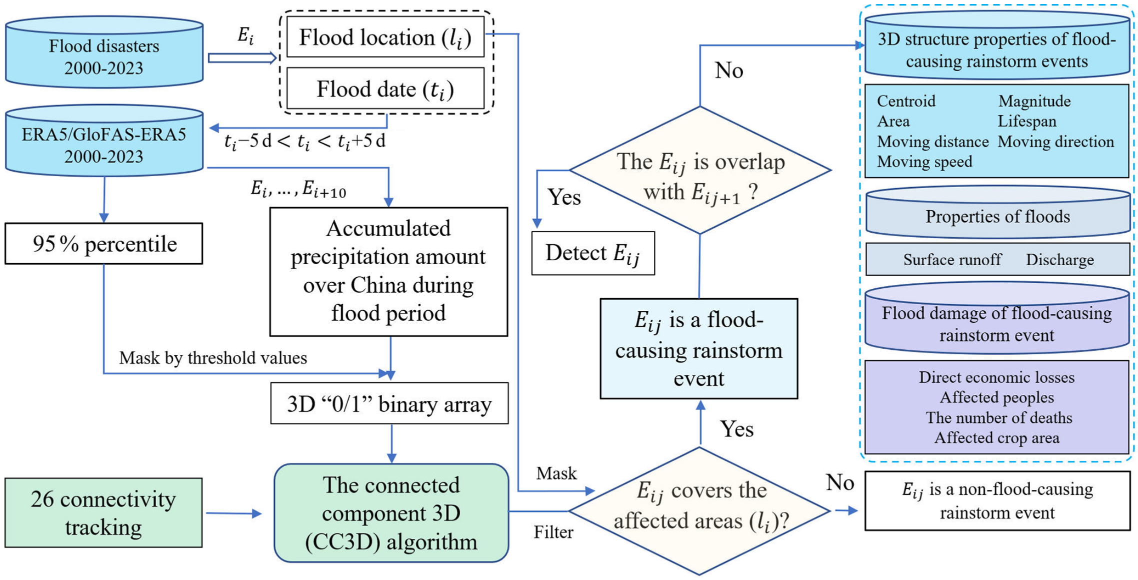

Figure 3. Flowchart of the precipitation event identification algorithm.

sons (from May to October) during 2000–2023. In our study, grid cells with accumulated amount of FCP event (E_i) less than threshold values are excluded from further analysis. Subsequently, we stored the hourly precipitation during start and end time of FCP event (E_i) in a 3D voxel array (i.e., latitude × longitude × time) in "0/1" binary format. Here, if there is a rainy hour at the pixel location marked in the last step, it will be labeled "1"; otherwise, it will be labeled "0". This detection method is based on the connected component 3D (CC3D) algorithm (Silversmith, 2021). The CC3D algorithm is the freely available Python package connected-components-3d (https://pypi.org/project/connected-components-3d/, last access: 19 August 2026). The "0/1" binary array is input into the CC3D algorithm to identify all possibly connected voxels with a 26-connectivity criterion. The CC3D algorithm can move to a 26-connected neighbourhood, and searches for all 26-connected components in a 3D array along the dimensions of latitude, longitude, and time. The 26-connectivity search enables a contiguous precipitation event at a grid in the current hour to move to adjacent grids in the following hour. This configuration ensures that different contiguous precipitation events E_i do not be overlapped or touched in the space. As a result, E_i contiguous precipitation events are retained during start and end time of FCP event (E_i). If the flood-affected area is covered by the contiguous precipitation event E_i, E_i is classified as a flood-causing precipitation event.

3. Determining the independence of FCP event: To ensure the FCP event (E_{ij}) is an independent event (i.e., E_{ij} is neither spatially adjacent nor temporally contiguous), we utilized the CC3D algorithm to forward-detect the next 10 flood records (i.e., $E_{ij+1}, \ldots, E_{ij+10}$) for each E_{ij}. If any part of E_{ij} not spatial overlaps with any part of events (i.e., $E_{ij+1}, \ldots, E_{ij+10}$), E_{ij} is classified as an independent event. If the overlap ratio exceeded 50 % between event E_{ij} and other events (i.e., $E_{ij+1}, \ldots, E_{ij+10}$), time interval between the events is more than 2 d, and they are from different precipitation types (e.g., TC and non-TC. The China Meteorological Disaster Yearbook (MDY) classifies flood events into TC and non-TC during 2000–2020, while the supplementary flood disaster data from 2020 to 2023 are categorized into TC and non-TC based on the official disaster bulletins and authoritative news reports), E_{ij} is considered as an independent event.

Based on the above FCP identification processes, 1041 flood disaster records were grouped into 632 independent precipitation events, comprising 386 non-TC events and 246 TC events.

3.3 Calculating the 3D structure properties of contiguous FCP event

For each contiguous FCP event identified by the previous step, the 3D structural properties can be characterized by the following multidimensional metrics, and shown in Fig. 4a–b, consistent with previous studies (Wang et al., 2022a, 2025):

1. Accumulated magnitude: The sum of the precipitation amount over all grid cells across all hours of the FCP event.

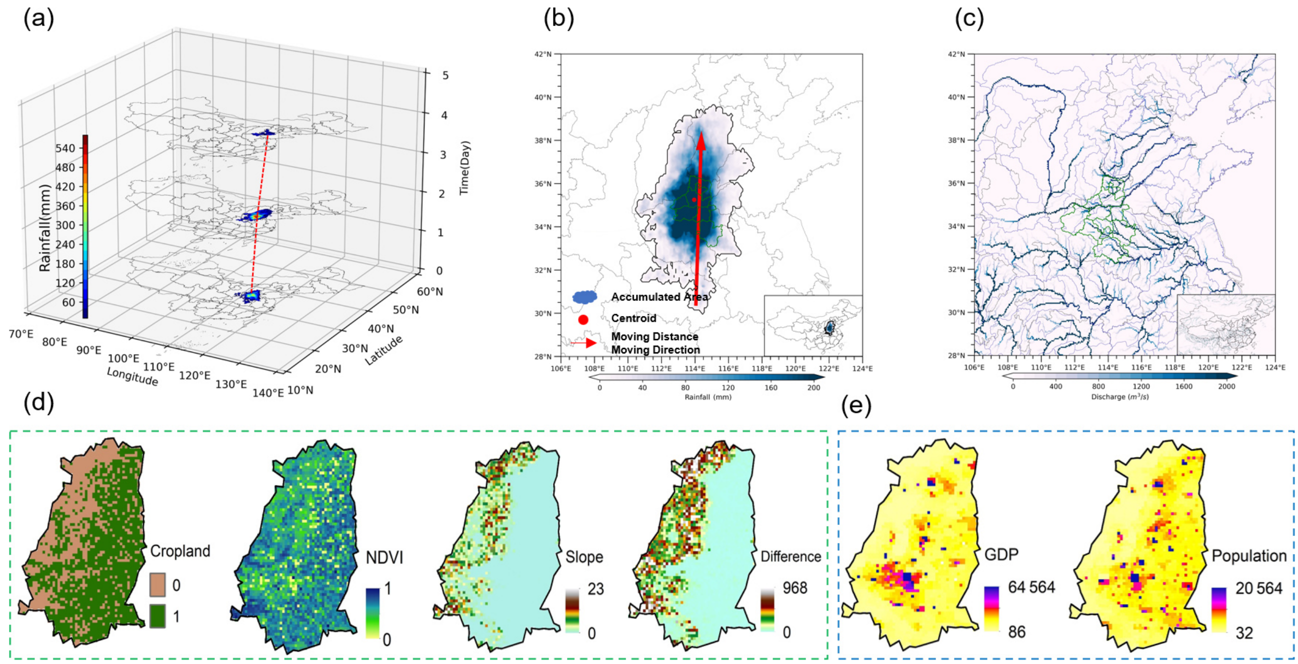

Figure 4. **(a)** Three-dimensional (3D) evaluation of a spatiotemporally contiguous FCP event that occurred on 21 July 2021 in Henan of China. **(b)** The evaluation features of FCP event. The shading denotes the FCP accumulated area. The red dot denotes the centroid of contiguous FCP event. The red arrow represents the movement of FCP event, the moving direction is from the tail to the head of the arrow, and the length of arrow indicates moving distance. The green polygons show the disaster-affected prefecture-level administrative units. **(c)** The river discharge during the FCP period. The green polygons show the disaster-affected prefecture-level administrative units. **(d)** The human activity factors (including population and GDP) in the heavy rainfall coverage areas of FCP event occurred on 21 July 2021 in Henan of China. **(e)** The environmental factors of Earth's surface, including cropland, NDVI, slope, and elevation difference, in the heavy rainfall coverage areas of FCP event occurred on 21 July 2021 in Henan, China.

2. Accumulated affected area: The horizontal projected area on the land surface affected by the FCP event.
3. Centroid: Represents the position of precipitation in the 3D space (latitude × longitude × time), calculated as the weighted center of FCP event within 3D space.
4. Lifespan: The time interval from the centroid at the start to the centroid at the end of the FCP event.
5. Moving direction: The azimuth angle pointing from the centroid of the begin time to the centroid of the end time.
6. Moving distance: The maximum distance across all hourly centroids during FCP event period.

3.4 Calculating the hydrological, environmental, and anthropogenic impact factors within FCP affected areas

Based on the accumulated affected area of FCP events presented in Sect. 3.3, the vector shapefile of the flood-affected areas is utilized as a spatial mask to extract hydrological, environmental, and anthropogenic factors within FCP affected areas (Fig. 4c–e). In this study, eight factors are selected to quantify the relationship between extreme precipitation characteristics and flood disasters across China. Detailed calculation methods are summarized in Table 2.

3.5 Geographical detector model

The geographical detector model is a set of statistical methods to explore spatial heterogeneity of explanatory variables, reveal interactions between driving factors, and quantify contribution rate of individual drivers (Wang and Hu, 2012). The formulas for ecological detection, risk detection, interaction detection, and factor detection were given in Wang et al. (2010). The core principle of factor detection is to determine whether the independent variable can explain the dependent variables and to investigate whether the interaction of two independent variables enhances, diminishes, or has no effect on the dependent variable. The results of interaction detector between two independent variables are classified into five types shown in Table 3. By comparing the q value of each factor and the q value of the two factors superposition, the geographical detector can determine whether there is an interaction between two factors, and whether their interaction is linear or nonlinear. Generally, $q \in [0, 1]$, q value is close to 1, meaning the independent variables has a strong influence

Table 2. Hydrological, environmental, and anthropogenic impact factors within FCP affected areas.

Category	Factors	Unit	Description
Hydrological processes	Surface runoff	mm	Total surface runoff within the FCP affected areas during the FCP event.
	River discharge	$m^3\ s^{-1}$	Difference between the peak flood discharge within the FCP affected during the FCP event and the pre-event base discharge.
Environmental characteristics	Cropland	ha	Total cropland coverage area within the FCP affected areas during the FCP event.
	NDVI	–	Mean NDVI value within the FCP affected areas during the FCP event.
	DEM Slope	°	Mean terrain slope within the FCP affected areas during the FCP event.
	DEM difference	m	Mean DEM difference within the FCP affected areas during the FCP event.
Human activities	GDP	CNY	Total GDP within the FCP affected areas during the FCP event.
	Population	Person	Total population within the FCP affected areas during the FCP event.

on independent variables, while a q value is close to 0, indicating that the dependent variable is spatially randomly distributed. Detailed theoretical descriptions of the geographical detector model can be found in Wang and Hu (2012). The formula for the q value is depicted as follows:

$$q = 1 - \frac{1}{N\sigma^2}\sum_{i=1}^{n} N_i \sigma_i^2 \quad (1)$$

where, $i = 1, \ldots, n$ represents the stratification for variable factor; N and N_i denote the total number of the units in the whole region and in stratum i, respectively; σ_h^2 and σ^2 are the variances of the dependent variable Y within N_i and N, respectively.

Referring to Liu et al. (2018), ten variables related to precipitation, the land surface environment conditions, and human activities were selected to determine the main factors influencing the spatial distribution of flood disasters. The precipitation variables can be characterized by the 3D structure properties of contiguous FCP event, including accumulated area, accumulated magnitude, lifespan, and moving distance. It is to be noted that the environment of the land surface (i.e., cropland, NDVI, slope of terrain, and elevation differences of terrain) and human activities (i.e., population and GDP) variables are represented by average values within the FCP event affected areas, as illustrated in Fig. 4c and d.

3.6 The scatter degree method

The scatter degree method (SDM) is an objective evaluation method that reflects the overall differences among evaluated objects. The basic principle of SDM is to select weight coefficient for indicators so that the difference among evaluated objects is maximized. Therefore, deriving weight coefficients for each indicator based on their intrinsic importance is critical. In our study, the SDM is employed to determine the weight of each indicator and calculate the comprehensive evaluation index for flood disaster and their driving factors, as the following steps:

Assume that the comprehensive evaluation function for y can be expressed as:

$$y = \omega_1 o_1 + \omega_2 o_2 + \ldots + \omega_m o_m = \boldsymbol{w}^{\mathbf{T}} \boldsymbol{O} \quad (2)$$

where, $\boldsymbol{w} = (\omega_1, \omega_2, \ldots, \omega_m)^T$ denotes the weight coefficient vector, $\boldsymbol{O} = (o_1, o_2, \ldots, o_m)^T$ represents the standardized evaluated object vector.

According to the SDM method, let $\mathbf{H} = \boldsymbol{O}^T \boldsymbol{O}$, which is a real symmetric matrix. By calculating the eigenvalues of $\mathbf{H}$, we can obtain the standard feature vector of maximum eigenvalue. Finally, the weight ω_i for each sub-risk indicator is obtained from this eigenvector. Subsequently, put ω_i into Eq. (2), the comprehensive evaluation index of flood disaster and their driving factors is computed.

4 Results

4.1 Spatial distribution of contiguous FCP events in China

Significant contrasts exist in flood characteristics induced by TC and non-TC rainstorm (Lu et al., 2020). In this study, 632 FCP events are classified into 246 TC and 386 non-TC precipitation events, and their 3D structural properties across China are shown in Fig. 5. The centroids of an FCP events represent the geographical location, as shown in Fig. 5a and b. The centroid size and color denote the

Table 3. Types of interaction between two independent variables.

Interaction types	Description
$q(AB) < \min(q(A), q(B))$	The q nonlinearly weaken after the interaction.
$\min(q(B), Q(A)) < q(AB) < \max(q(A), q(B))$	The q uniformly weaken after the interaction.
$q(AB) = q(A) + q(B)$	The A and B stand independent.
$q(AB) > \max(q(A), q(B))$	The q linear enhancement after the interaction
$q(AB) > q(A) + q(B)$	The q nonlinear enhancement after the interaction.

Note: $\min(q(A), q(B))$ means the minimum value of $q(A)$ and $q(B)$. $\max(q(A), q(B))$ means the maximum value of $q(A)$ and $q(B)$.

accumulated area and magnitude, respectively. TC-induced rainstorm events mostly occur in the coastal areas of China, with the majority concentrated in coastal regions of Southern China (SC) rather than Northern China (NC) (Fig. 5a). These events have an average affected area of 9.63×10^2 km^2 and accumulated magnitude of 3.95×10^4 mm. Notably, TCs that moved farther inland exhibit larger accumulated areas and magnitudes, especially in northeastern NC.

Figure 5c shows the spatial distribution of the migration of TC-induced FCP events. The arrow color represents the lifespan of the FCP events, the length of the arrows represents migration distances of FCP events, and arrow is the direction of the migration of FCP event. On average, TC-induced FCP event persists for 22.84 h and travels 396.99 km. TC-induced FCP events are more inclined to move to the westward, which is consistent with an earlier study (Zhang et al., 2013). The westward shift of the western Pacific subtropical high (WPSH), westward steering flow, and easterly vertical wind shear are the main drivers of the formation of the TC moving westward (Wang et al., 2022). Meanwhile, some TCs prefer to shift northward or northeastward due to the eastward shift of WPSH, westerly vertical wind shear, weak mountainous blocking and westerly steering flow surrounding the TCs (Wang et al., 2022).

Figure 5b shows the centroids of non-TC-induced FCP events. It can be observed that non-TC-induced FCP events are mainly clustered in SC and NC. The average accumulated magnitude and projected area are 4.45×10^4 mm and 1.52×10^3 km^2, respectively. The non-TC events with larger accumulated magnitude and projected areas are mainly distributed in center of SC and NC. In contrast, the magnitude and affected area of non-TC events is larger than the TC events. The migration characteristics of non-TC events are illustrated in Fig. 5d. It is seen that the non-TC events are more inclined to move eastward, which is mainly attributed to the mid-latitude climatological westerlies and southwesterly monsoon circulation (Wang et al., 2022). These eastward moving FCPs have an average traveling distance of 489.58 km and lifespan of 21.63 h, which is slightly longer than TC-induced events. This finding is consistent with research by Wang et al. (2022), that suggested that FCP events with more persistent lifespan tend to travel longer and exhibit larger accumulated magnitudes and projected areas.

4.2 Temporal changes of contiguous FCP events in China

Figure 6 illustrates the long-term trends of multidimensional metrics of contiguous FCP events in China during 2000–2023. All metrics of contiguous FCP events show positive trends, consistent with findings from Li and Zhao (2022). The intensification of extreme precipitation is primarily governed by the thermodynamic effects constrained by the Clausius-Clapeyron (CC) relationship. When atmospheric temperature increases, saturation vapor pressure increases at a theoretical rate of 6–7 % °C^{-1}, providing the fundamental physical mechanism for enhanced extreme precipitation events (Trenberth et al., 2003; Allan et al., 2022). The accumulated area and magnitude of FCP events show slight increasing trends, with an annual variation of 0.15×10^2 km^2 yr^{-1} and 0.07×10^4 mm yr^{-1} (insignificant at the 0.05 level), respectively (Fig. 6a and b). The lifespan of FCP events shows an increasing trend at a rate of 0.12 h yr^{-1} (Fig. 6c), and the total traveling distance exhibits an upward trend at a rate of 0.38 km yr^{-1} (Fig. 6d). By contrast, a notable observation is that the non-TC events generally exhibit larger accumulated areas and magnitudes, as well as longer lifespans and moving distances, than TC events. Meanwhile, the uptrend trends of metrics of non-TC events are more pronounced than those for the TC events. This indicates that non-TC events have more pronounced and widespread impacts compared with TC events.

4.3 Spatiotemporal variations of surface runoff and discharge during the FCP events periods

The spatial and temporal variations of hydrological processes during the FCP event periods are analysed (Figs. 7 and 8). It can be seen from Fig. 7 that FCP events associated with low surface runoff are found mainly in Northwestern China (NWC) and the Qinghai-Tibetan Plateau (TP). At the same time, FCP events with low surface runoff are distributed in the western parts of SC and NC. By contrast, FCP events with high surface runoff are predominantly observed in central SC and NC and northeastern NC. A comparison between TC and non-TC events reveals that the average surface runoff of non-TC FCP events is 30.81×10^3 mm, which is higher than that of TC FCP events with average value of 23.34×10^3 mm. Fig-

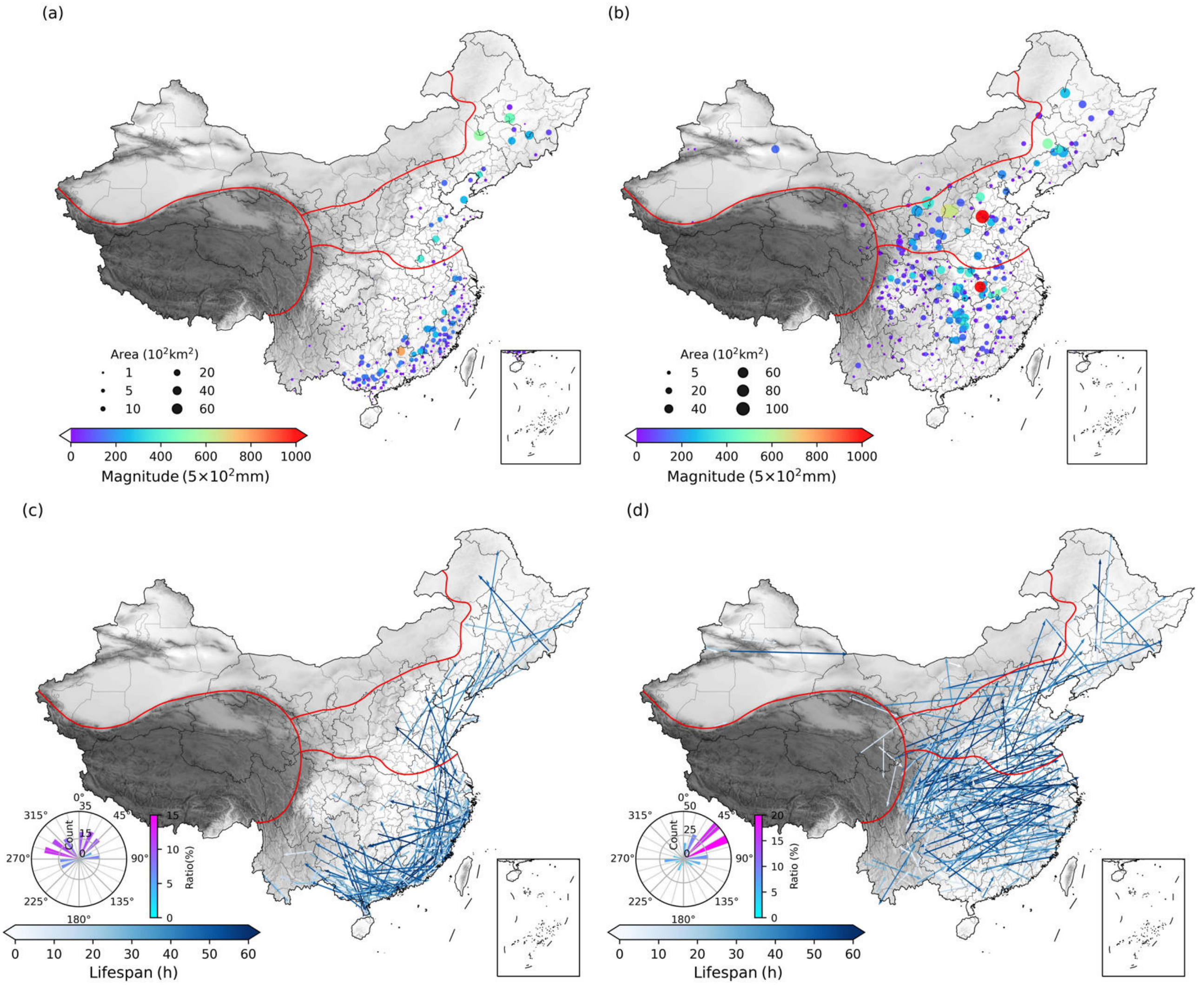

Figure 5. (a) and **(b)** show the spatial distribution of the overall centroids of TC and non-TC FCP events in China during 2000–2023, respectively. The color and size of the circle indicate their accumulated magnitude and area, respectively. **(c)** and **(d)** depict the spatial movement of the TC and non-TC FCP events in China, respectively. The colors represent the lifespan. The arrow indicates the movement direction. The rose diagram illustrates the directional distribution of FCP in China, with color indicating the ratio of current direction to total events. The shading indicates the terrain height.

ure 7b presents a similar spatial variation of river discharge. FCP events with high river discharge are primarily concentrated in the central of SC, NC, and northeastern parts of NC. These findings indicate that regions with large surface runoff and river discharge in the central SC and NC face a higher probability of flood occurrence.

Figure 8a and b illustrate the temporal variations of surface runoff and river discharge during FCP event periods, respectively. Both surface runoff and river discharge show increasing trends, yet the trend is not significant at the 0.05 level. The mean surface runoff and river discharge for non-TC FCP events are higher than that of TC events. This finding can be attributed to the increase of precipitation features in China, as shown in Fig. 5. According to the correlation analysis between the accumulated magnitude of FCP events and surface runoff and river discharge, we find that surface runoff exhibits a significant correlation with accumulated magnitude ($R = 0.87$, $P < 0.001$). The correlation coefficients between the accumulated magnitude and surface runoff are 0.85 for non-TC and 0.93 for TC FCP events, both of which are statistically significant at the 0.01 level (Fig. 8c). By contrast, the correlation between accumulated magnitude and river discharge is relatively weaker, with the mean correlation coefficient greater than 0.67 and statistically significant at the 0.05 level. Consequently, enhanced 3D characteristics of FCP events across China drive increases in surface runoff and river discharge. Particularly, floods are more prominent in central SC and NC.

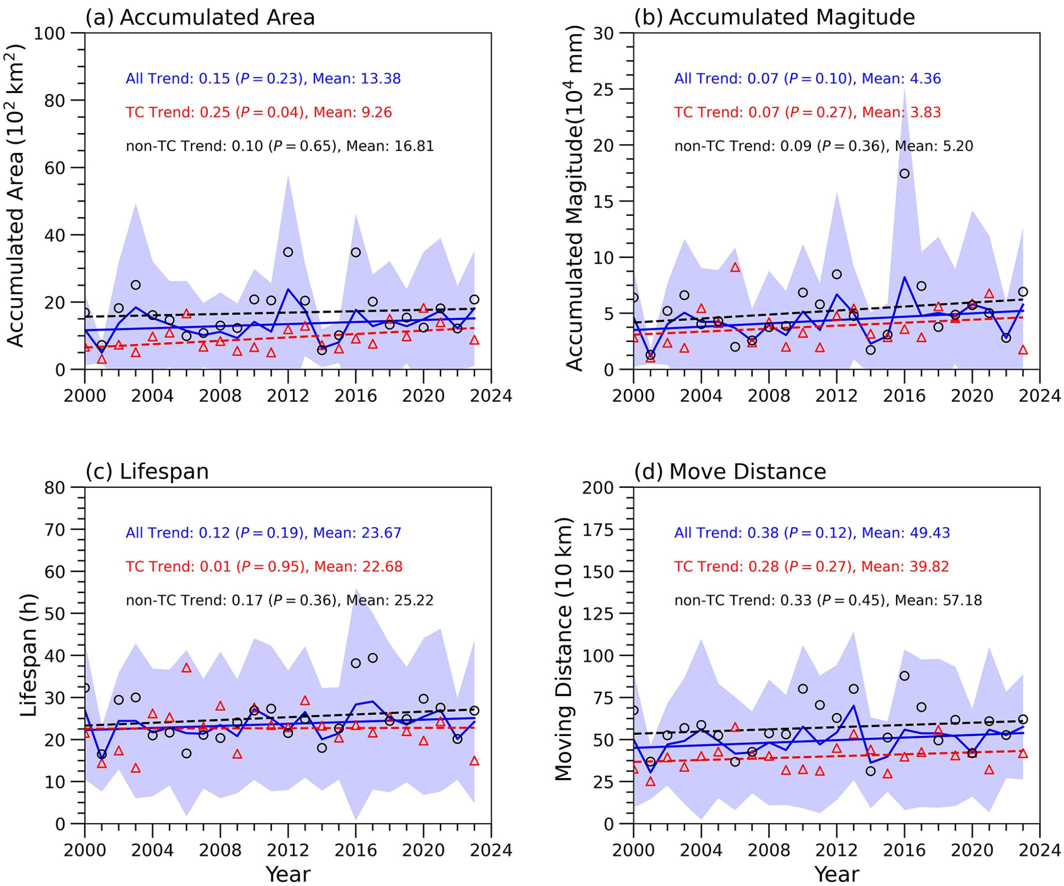

Figure 6. Time series of annual mean metrics of FCP event in China during 2000–2023: **(a)** accumulated area, **(b)** accumulated magnitude, **(c)** lifespan, and **(d)** moving distance. The blue solid line and straight line indicate the temporal evolution and trend of mean values of FCP during 2000–2023, respectively. The blue shading indicates the ± standard deviation across the evolution of total FCP events. The black dots and dashed line represent the annual mean values and trend of non-TC FCP events during 2000–2023, respectively. The red triangles and dashed line represent the annual mean values and trend of TC FCP events during 2000–2023, respectively.

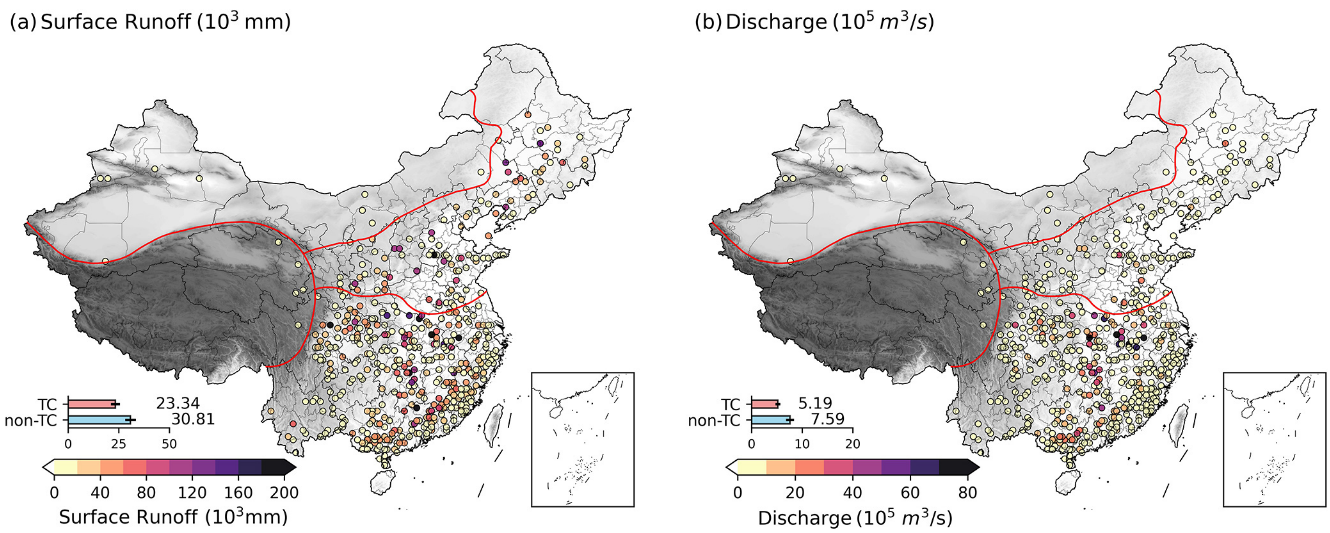

Figure 7. Spatial distribution of **(a)** surface runoff and **(b)** discharge during FCP event periods in China from 2000 to 2023. Bar chart illustrates the mean values of surface runoff and river discharge for TC and non-TC FCP events. The shading indicates the terrain elevation.

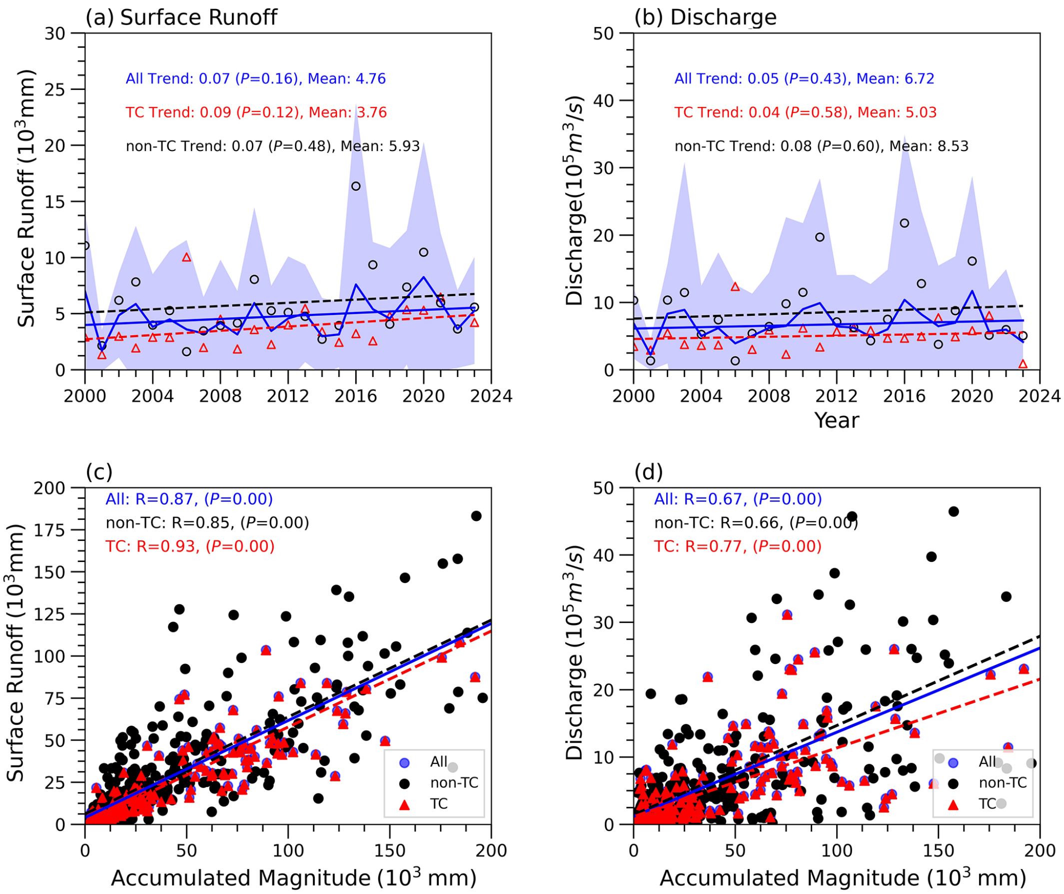

Figure 8. Time series of annual mean values of surface runoff **(a)** and river discharge **(b)** during FCP event periods in China from 2000 to 2023. The blue solid line and straight line indicate the time evolution and trend of mean values of surface runoff and discharge during 2000–2023, respectively. The blue shading indicates the ± standard deviation across the evolution of surface runoff and discharge during FCP events. The black dots and dashed line represent the annual mean values and trend of surface runoff and discharge during the non-TC FCP period from 2000 to 2023. The red triangles and dashed line represent the annually mean values and trend of surface runoff and discharge during the TC FCP period from 2000 to 2023, respectively. The relationships between surface runoff and accumulated magnitude, and between discharge and accumulated magnitude are shown in **(c)** and **(d)**, respectively. Black dots represent the non-TC events, red triangles represent the TC events, and the regression lines indicate the correlation trends (solid blue line for all events, dashed red line for TC events, and dashed black line for non-TC events). The Pearson correlation coefficient (R) and significance level (P) are provided for each category, showing significant positive correlations between the hydrological variables and accumulated magnitude at the 99 % confidence level.

4.4 Spatial distribution of flood disaster in China

Figure 9 illustrates the spatial distribution of the flood affected population, death, direct economic loss, and affected cropland areas in China during 2020–2023. The geographical location of each flood event is represented by the centroid of the corresponding precipitation events. It can be easily observed from Fig. 9a that FCP events occurring in the SC and parts of the NC are mostly associated with larger affected population, whereas the flood-affected population in NWC and Qinghai-Tibetan Plateau (TP) is relatively low. Different spatial patterns can be found for the number of deaths caused by FCP events (Fig. 9b) across China when compared to that of flood-affected population (Fig. 9a). Higher number of deaths are observed in the SC and NC, but the number of deaths is fewer in the center of SC. Besides, the number of deaths is relatively large in the NWC and the surrounding regions of TP. The direct economic losses caused by FCP events are more severe in the southeastern and western parts of SC, as well as the central and northeastern regions of NC (Fig. 9c). For cropland, the affected cropland areas are mainly distributed in southeastern regions of SC and central and northeastern regions of NC (Fig. 9d). Besides, among these FCP events, TC-induced flood result in more severe disasters than non-TC-induced events.

To further investigate the flood-affected rate within the coverage areas of FCP events, we calculated the ratios of flood affected population, deaths, direct economic loss, and affected cropland areas to the total population, GDP, and total cropland within the coverage areas of FCP events, respec-

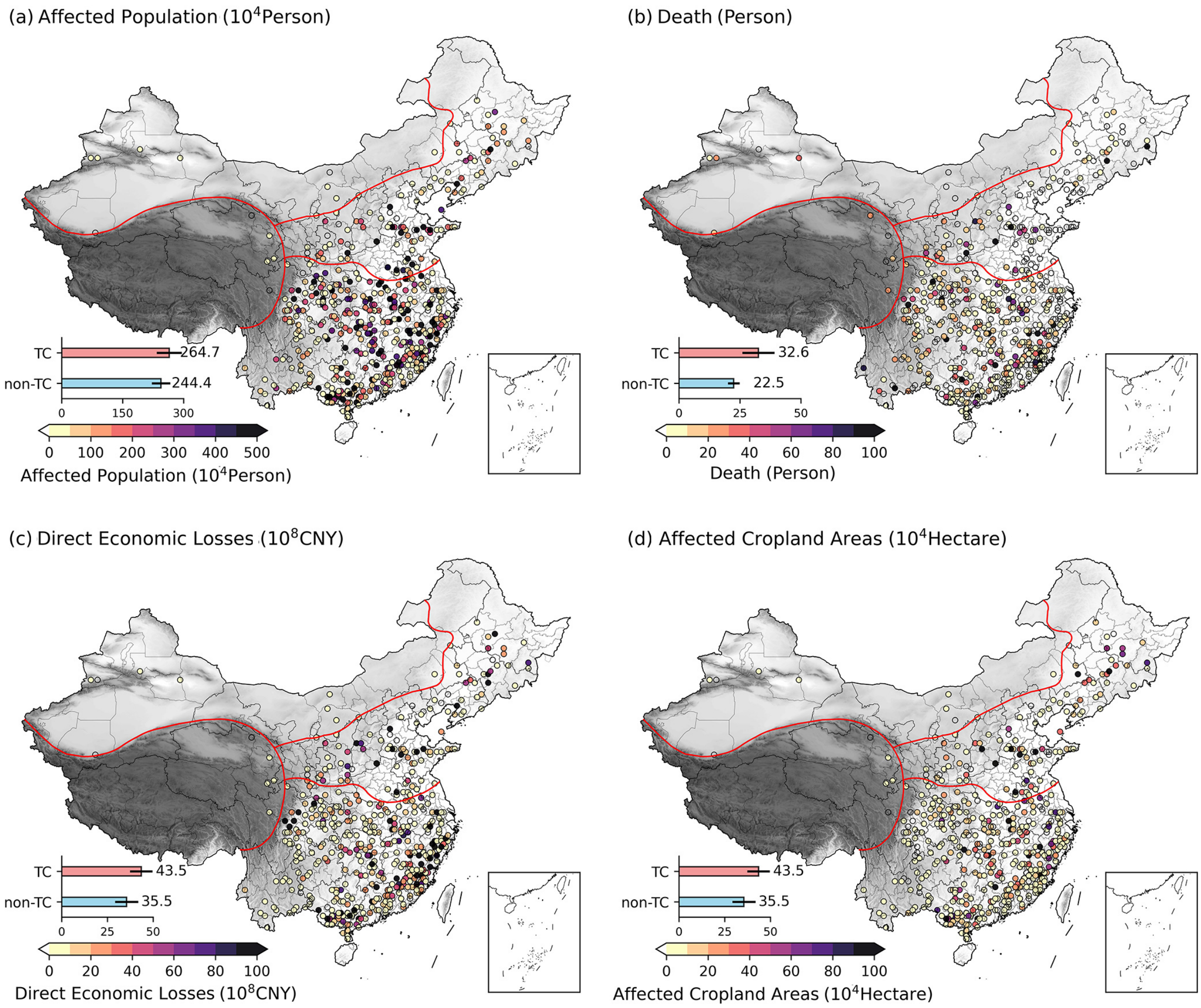

Figure 9. Spatial distribution of **(a)** flood affected population, **(b)** death, **(c)** direct economic losses, and **(d)** affected cropland areas in China during 2000–2023. Bar chart illustrates the mean values of flood disaster of TC and non-TC FCP events. The shading indicates the terrain height.

tively (Fig. 10). As shown in Fig. 10a, high ratios of flood affected population to the total population within the coverage areas of FCP events are predominantly concentrated in SC, which is similar to the affected population distribution in Fig. 9a. However, high death rates are primarily distributed in the southeastern fringe of the TP and southwestern China (Fig. 10b). This phenomenon can be attributed to the high population density and robust economic development in eastern and southern China, and enhanced flood mitigation capacity to mitigate floods impacts by the construction of levees and flood-mitigated infrastructures (Fang et al., 2018). In contrast, mountainous areas in the southeastern fringe of the TP and southwestern China lack such infrastructures. FCP events in these regions often trigger sudden-onset flash floods accompanied by landslides and debris flows, severely threatening human lives (Chen et al., 2021). For the direct economic loss, the ratio to the total GDP is low in the southeastern SC, but relatively high in the western SC and northeastern NC. This suggests that FCP events caused significant economic losses in the western SC, rather than eastern SC with relatively high GDP. Regarding affected cropland, the smaller absolute affected cropland areas but larger ratio of affected cropland to the total cropland within the coverage areas of FCP event can be found in the coastal areas of SC. This is because this region frequently experiences TC rainfall processes, which often coincide with strong winds and storm surges, posing severe threats to the cropland. Overall, flood disasters caused by FCP in China exhibit the changing characteristics of “high impact-low losses ratio” in SC and NC and “low impact-high losses ratio” in TP and SWC.

4.5 Temporal changes of flood disaster in China

Figure 11 shows the time series of the flood disasters in China during 2000–2023. As shown in Fig. 11a, the flood-affected

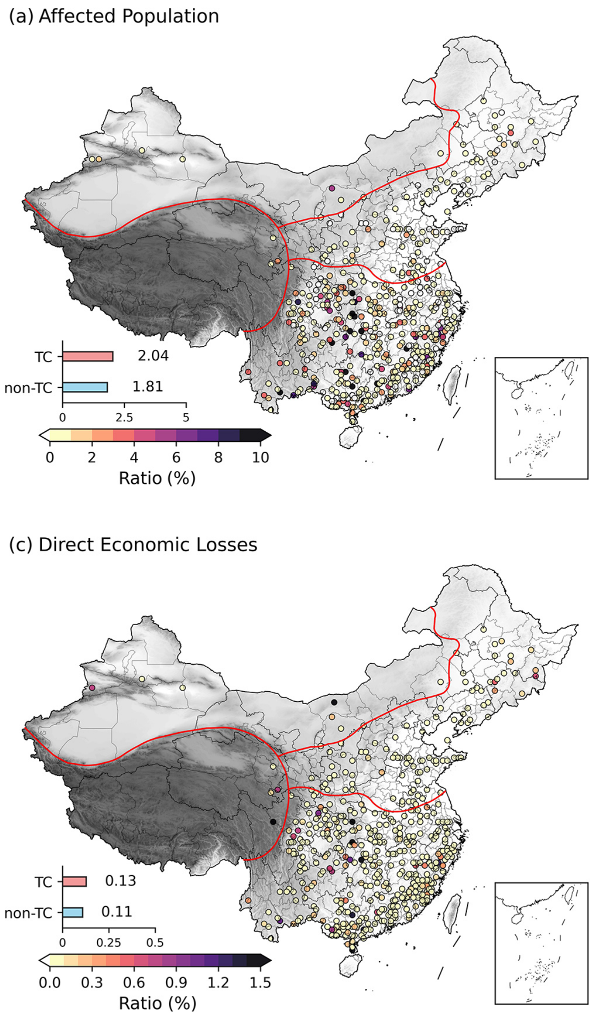

Figure 10. Spatial distribution of **(a)** the ratio of flood affected population to the total population within the coverage areas of FCP event, **(b)** the ratio of death to the total population within the coverage areas of FCP event, **(c)** the ratio of direct economic losses to the total GDP within the coverage areas of FCP event, and **(d)** the ratio of affected cropland area to the total cropland area within the coverage areas of FCP event in China. Bar chart illustrates the mean values of the ratio of flood disaster of TC and non-TC FCP events. The shading indicates the terrain height.

population and the ratio of affected population to total population within the coverage areas of FCP events show a clear decreasing trend. The TC-induced affected population declines by 14.95×10^4 persons per year, which is larger than the non-TC event with 12.09×10^4 person per year (significant at the 95 % confidence level). The number of deaths also shows a decreasing trend during the period, except for extremely severe floods in 2016 and 2019. For the time being, we note that the TC-induced deaths decreased significantly by about 1.27 persons per year ($P < 0.05$) from 2000 to 2023. A similar temporal pattern is observed for flood affected cropland areas in Fig. 11d, although there are differences in various of severe flood years after 2010. These results suggest that flood disaster represents a significant reduction trend in the past twenty years in China, despite there appear fluctuation features after 2010 due to extreme precipitation events, e.g., extreme rainfall in July 2016 affected 10.44 million people, caused 225 lives death, and resulted in economic losses of USD 57.46 billion. However, it is interesting that temporal trend of the direct economic losses from FCP event is completely different compared to other flood disasters metrics. Prior to 2010, flood caused direct economic loss is generally declined, then shifted to an increasing trend, and subsequently fall back into decrease. Notably, the trends of direct economic losses induced by TC and non-TC events are not statistically significant. In fact, previous studies have shown that economic development is correlated with the increase in direct economic losses (Wu et al., 2018). However, our analysis here suggests heterogeneous temporal changes in the decreasing trend in direct economic losses after 2010. This indicates that the direct economic loss varies with different levels of economic development.

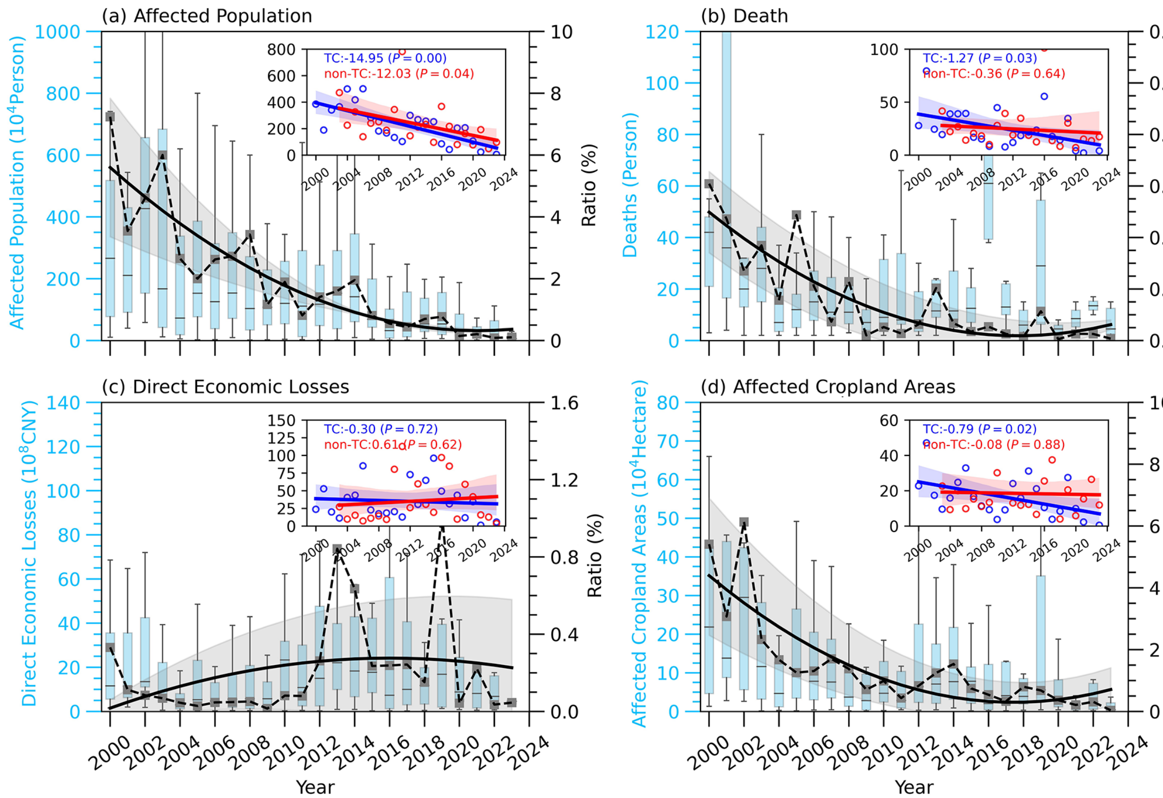

Figure 11. Time series boxplot (left y-axis) of **(a)** flood affected population, **(b)** death, **(c)** direct economic losses, and **(d)** affected cropland areas in China from 2000 to 2023. Time series of ratio (right y-axis) of **(a)** flood affected population, **(b)** death, **(c)** direct economic losses, and **(d)** affected cropland areas to total population, GDP, cropland within the coverage areas of FCP events. The black dashed line represents annual mean ratio. The shaded gray area represents the 95 % confidence interval on the basis of the quadratic fitted line (black line). Annual mean values and trends of flood (red and blue show the non-TC and TC FCP events, respectively) affected population, death, direct economic loss, and affected cropland areas over China from 2000 to 2023 shown in four subregions.

4.6 Analysis of driving factors of flood disasters

Figure 12 displays the Pearson correlation coefficients (CC) between flood disasters and their driving factors. Flood disasters have a significant positive correlation with precipitation factors ($P < 0.001$), except for the number of deaths, which shows a weak correlation. Among the precipitation factors, accumulated magnitude and lifespan show higher CC values with flood disasters, indicating that precipitation events with larger accumulated magnitude and longer lifespan tend to trigger more severe flood disaster impacts (Fig. 12a and e). Significant positive correlations between flood disasters and surface runoff and river discharge are found in Fig. 12b and f, revealing that high surface runoff and river discharge are critical factors to trigger flood disasters. Concurrently, human activity factors (i.e., GDP and population) also have positive correlation with flood disasters ($P < 0.001$), suggesting that flood disaster effect caused by FCP is more serious in high economically developed and densely populated areas (Fig. 12d and h). Considering the relevance of the environment factor and flood disasters, cropland area shows positive correlation with the flood disaster, and NDVI exhibits a weak positive correlation with all flood disaster and not passing the significance test at 0.05. The result shows that flood-caused destruction of cropland leads to severe economic losses, while the changes in NDVI have a limited impact on flood disasters is limited. In contrast, slope and difference in elevation show weak negative correlatives with flood disaster, except for the number of deaths. This is because the most population and economically developed regions are predominantly distributed in the low-altitude areas of the eastern regions in China. However, mountainous areas experience relatively higher numbers of flood-related deaths leading to a positive correlation between flood disasters and altitude (Fig. 12c and g).

To further identify the key driving factors influencing the changes in flood disasters, based on the experience of previous research (Liu et al., 2018), we conducted an interaction detection based on Geodetector method in Fig. 13. When comparing the q value of each single factor, precipitation and hydrological factors have the greatest explanatory power for the flood disasters, followed by the human activity factors, and the environmental factors have the lowest explanatory

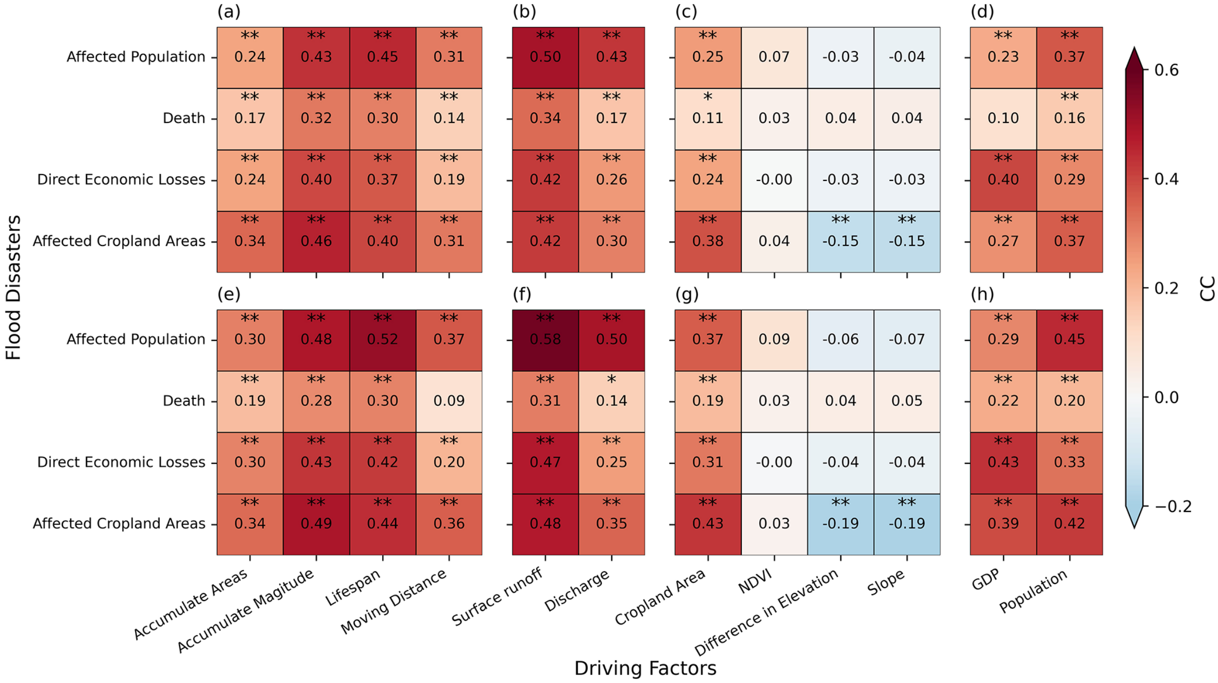

Figure 12. Heatmap showing the Pearson's correlation coefficient (CC) between flood disasters (flood affected population, death, direct economic losses, and affected cropland areas) and flood driving factors (3D precipitation features (accumulated area, accumulated magnitude, lifespan, and moving distance), hydrology factors (surface runoff and river discharge), environmental factors (cropland area, NDVI, slope, and difference elevation), and human activities (population and GDP) factors). Significance correlations are marked by asterisk, $^{*}P < 0.01$; $^{**}P < 0.001$.

power. This suggests that the flood disasters are overwhelmingly determined by the precipitation features, land surface hydrological processes, and human activities factors, which is consistent with findings from previous studies (Wang et al., 2022b). In all evaluation factors, the interaction q-values of any two factors are greater than those of the individual factors (Fig. 13), that is to say, the explanatory power of an individual factor may be enhanced when interacting with other factors. Specifically, the interaction between precipitation and hydrological factors and environmental factors displays significant nonlinear enhancement and bivariate enhancement effects. This means that although environmental factors have weak explanatory power on their own (Fig. 12c and g), their synergistic effects can exert a stronger influence due to nonlinear characteristics at different spatial and temporal scales. Therefore, the flood disasters in China are likely to be the result of a combination of factors.

To further reveal the spatial characteristics of interactions effect among driving factors on flood disaster, we calculated the comprehensive evaluation index of three driving factors based on the SDM method, and mapped the spatial distribution of dominant factors of flood disasters in Fig. 14. We found that precipitation and environmental factors have the largest spatial distribution among all potential driving factors, suggesting that flood disasters are influenced by combining precipitation and environmental factors in China. In the interim, the flood disasters events significantly influenced by the human activities are predominantly distributed in the center of SC and NC, which are densely populated regions in China (e.g., the middle-lower Yangtze River plain and the North China plain). This indicates that flood caused more severe disasters in densely populated areas, e.g., urban areas, which is consistent with our above findings presented in Fig. 12d and h.

5 Discussion

5.1 Analysis of flood-causing precipitation event features from a 3D perspective

Rainstorm is one of the most frequent natural hazards by triggering flooding and severe hazards in the world, seriously impacting populations, property, and socioeconomic development, thus, have garnered significant attention of the international society (Kharin et al., 2013; Ban et al., 2015; Wasko et al., 2021). In previous studies, the behaviours of rainstorms, such as frequency, intensity, and duration, have been extensively examined using maximum rainfall indices in specific regions (Fu et al., 2013; Deng et al., 2018). For example, Fu et al. (2013) constructed extreme rainfall indices and analysed spatial and temporal changes of extreme rainfall in China. However, these approaches only identified the con-

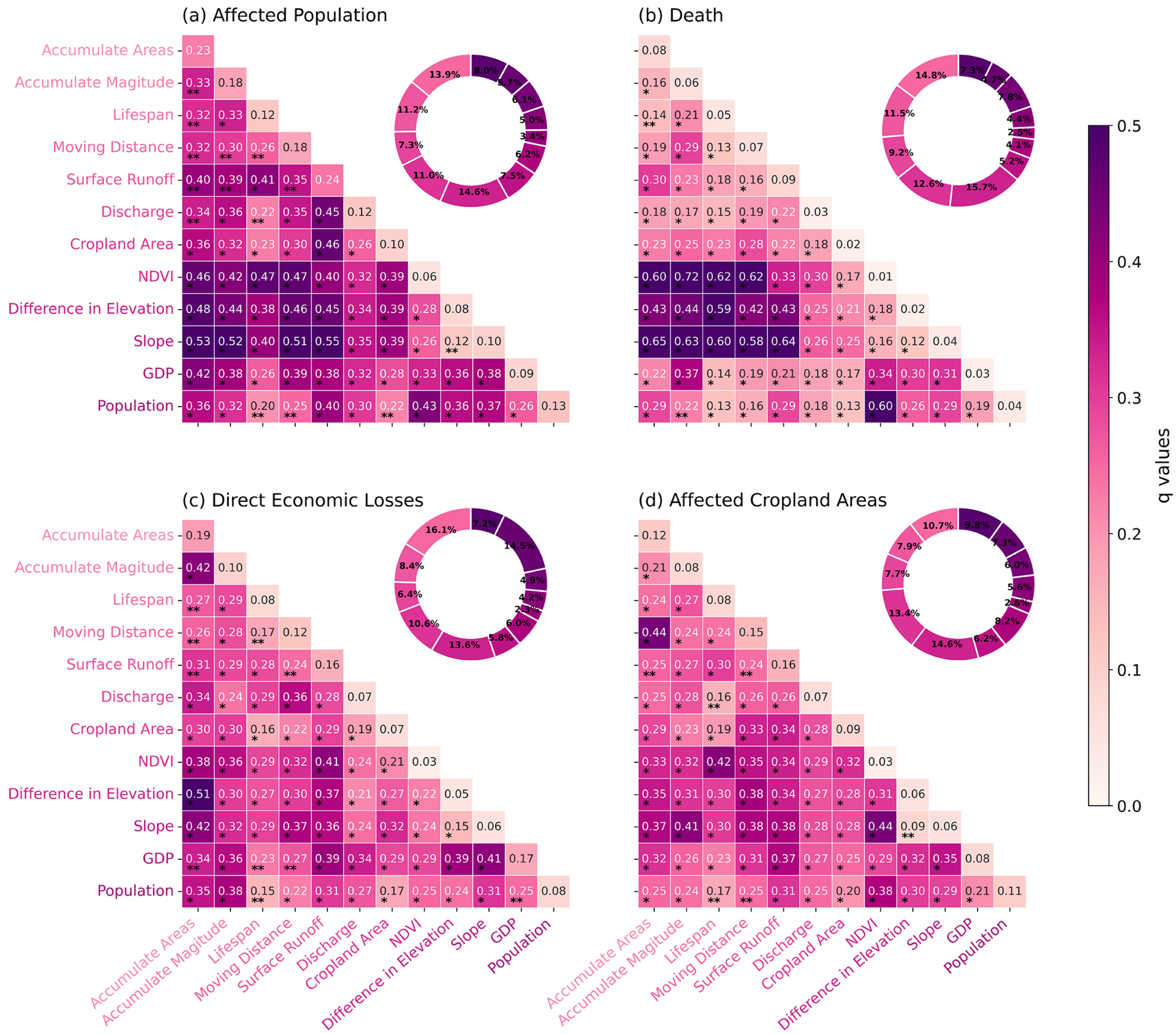

Figure 13. Interaction detection results of Geodetector analysis of driving factors: **(a)** for affected population, **(b)** for death, **(c)** for direct economic losses, and **(d)** for affected cropland areas. * indicates two-factor nonlinear enhancement; ** means two-factor bilinear enhancement. Pie charts in each subplot represent the contribution rations of each single factor.

tinuous rainstorm spatial features at two-dimensional (latitude × longitude) and examined temporal changes based on the time series of extreme rainfall index, while ignoring the synchronous spatiotemporal connections and independence of rainfall events. This oversight could lead to an irrational analysis of rainfall features over study area. To overcome this limitation, recently, Silversmith (2021) proposed an integrated spatial contiguity algorithm to characterize precipitation events at the spatial scale. Wang et al. (2022a) investigated the 3D characteristics of spatiotemporal contiguous extreme precipitation events in China, meanwhile, Wang et al. (2025) analysed the 3D evolutionary features of spatiotemporally contiguous flood-causing precipitation events using CC3D algorithm. Thus, view from a higher-dimensional perspective, the identified 3D precipitation features not only retain the features recognized through a lower dimensional perspective but also provide a more visual and stereo demonstration of the spatial moving process of precipitation events (Feng et al., 2024).

In this study, we attempted to extend the CC3D algorithm to investigate the 3D characteristics of precipitation events and conducted the first comprehensive assessment of flood disasters from the event-based perspective. To this end, we developed an automatic precipitation event recognition algorithm with the CC3D method as its core, as shown in Fig. 3. This method in our study provides a possibility to accurately determine the spatiotemporal contiguous flood-causing precipitation events and reveal their "true" 3D structures and

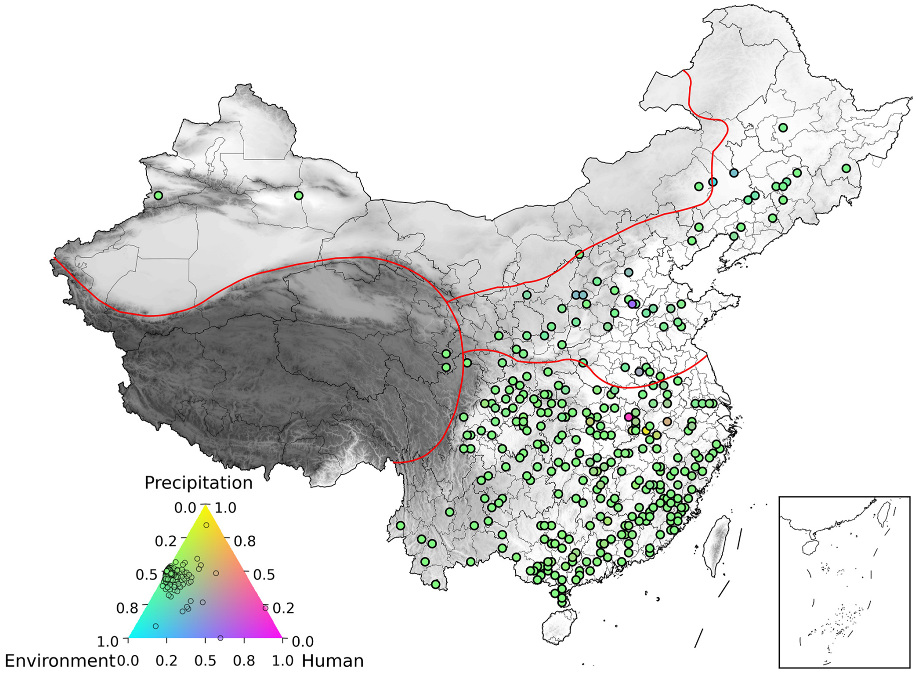

Figure 14. Ternary diagram shows the interannual trend of flood disasters, which is dominated by precipitation, environment, and human activities factors. The shading indicates the terrain height.

evolutionary patterns (e.g., moving direction, distance, and lifespan) from 2000 to 2023 in China. Additionally, the flood disasters caused by FCP events were extracted within the FCP event coverage areas, as illustrated in Fig. 4d, which could provide more reliable estimates of the influence of FCP events. Therefore, based on the above characteristics of events, our findings comprehensively reveal the characteristics of the precipitation and flood disasters from an event-based perspective. The results show that the FCP events were classified into 368 non-Tropical Cyclone (non-TC) and 246 TC events. TC-induced events, predominantly occurring in the coastal regions of Southern China (SC), have relatively small accumulated areas and magnitudes and short lifespan and moving distance, mostly inclined to move westward. In contrast, non-TC events are concentrated in SC and Northern China (NC), exhibiting eastward migration and characterized by larger accumulated magnitudes and affected areas and have a longer lifespan and moving distance than TC events. Thus, our research provided a new perspective for revealing the evolutionary features of spatiotemporally continuous flood-causing precipitation events from a 3D event-based perspective.

5.2 Potential driving factors of flood disasters in China

Precipitation, as a decisive factor of flood events, has attracted extensive attention from academia and policymakers. Many scholars have explored the spatiotemporal variability of extreme precipitation and its potential drivers in China. They suggested that the frequency of extreme precipitation events showed increasing trends and the relative contribution of extreme precipitation to the total precipitation also increased in most parts of China (Wu et al., 2019; Gu et al., 2022; Wang et al., 2022a; Fu et al., 2023). In comparison with these previous studies, our study introduces a new evaluation method, and comprehensively assesses the multi-dimensional characteristics of spatiotemporal FCP events. The results indicate that the accumulated area, accumulated magnitude, lifespan, and moving distance of FCP events are mostly increased during 2000–2023 (Fig. 6). This result is generally consistent with the trend of precipitation variation in China, and suggests that extreme precipitation events are projected to become more intense (Ban et al., 2015; Wu et al., 2019). These patterns are closely linked to the increase of the moisture-holding capacity of the atmosphere with higher temperature at approximately 7 % $^{\circ}C^{-1}$ (Trenberth et al., 2003). Under global warming context, the increasing atmospheric moisture and buoyancy not only elevate the frequency of extreme precipitation events but also can lead to intensification rates that exceed the Clausius–Clapeyron (CC) scaling, exhibiting super-CC scaling (Fowler et al., 2021). Under a +4 K warming scenario, probable maximum precipitation (PMP) events are projected to become substantially more frequent, with their annual exceedance probability rising by approximately 10^1–10^2 (Hiraga et al., 2025). Besides thermodynamic controls, dynamic factors associated with large-scale circulation changes also modulate the frequency and propagation of extreme rainfall by shifting storm trajectories and movement speeds (Chan et al., 2023; Wasko et al., 2024).

In contrast to the increasing trends and intensifying strength of extreme rainfall, flood disaster shows very mixed trends in China due to differences in analytical areas, data, and methods. For instance, Xie et al. (2018) pointed out that the combination of more frequent and stronger extreme rainfall and the rapid expansion of urban agglomeration is more likely to increase the flood risk in Nanjing metropolitan. Similar results were also found along the coast of China (Feng et al., 2023), the extreme precipitation events led to a corresponding increase in the risk of flooding. However, in our study, the flood disasters are inconsistent with extreme rainfall and flood, and represent a significant reduction in the past twenty years in China, except for the direct economic losses (Fig. 11), which has been confirmed by Wei et al. (2018). From the perspective of spatial distribution, FCP events with larger accumulated magnitude and projected areas caused larger flood are mainly distributed in the center of SC and NC, and cause more serious disaster losses, but the flood loss proportions are largely reduced. This discrepancy might be caused by larger-scale hydraulic projects, such as dams and reservoirs. By the end of 2018, there were 98 822 reservoirs existed in China, with a total storage capacity of 8.95×10^{12} m^3 (data are derived from China Water Statistical Yearbook 2018), which may significantly modulate the flood risks. Tang et al. (2023) studied the impact of dams on the flood in the Yangtze River, and found that dams and reservoirs mitigated the extreme flood by contributing to 94 % of the water level changes. In contrast, mountainous areas in the southeastern fringe of the TP and southwestern China, where the accumulated magnitude and projected areas of FCP events are relatively small, flood disaster proportions are large, especially the death (Chen et al., 2025). That means flash floods triggered by extreme rainfall events, representing a severe hazard in low-GDP regions. The robustness of the findings is supported by existing studies, suggesting that numerous engineering measures around the world have improved flood control standards and mitigated the rising risks of flash floods. Lim et al. (2018) analysed the global benefits of existing flood-control projects and identified an 8 % reduction in the exposed population and 7 % GDP property exposure losses per year in flood-inundated areas from 1986 to 2005. Zhao et al. (2022) indicated that reservoirs can decrease housing losses caused by flash floods by 9.7 %–45.7 %. In summary, flood disasters in China have been categorized into high-impact and low-loss in plain areas of SC, and low-impact and high-loss situation in the mountainous areas of west.

However, flooding is a complex physical process involving interactions among hydrology, meteorology, and land surface features that can be triggered by multiple mechanisms. Determining the factors that influence flood disasters from a multi-perspective is helpful for identifying the coupling mechanism between factors and flood disasters. We found that the anthropogenic activities (e.g., population and GDP) are the second most influential factor after extreme precipitation, which corresponds to previous literature reporting a positive relation between flood disasters and population, indicating that large populations in flood-affected areas are expected to have large flood risk exposure (Rogers et al., 2025). Our further examinations demonstrate the interaction between precipitation and environmental factors that displays significant nonlinear enhancement and bivariate enhancement effects, suggesting that precipitation situation and the topographical features of rainstorm area will have a major impact on the evolution of the flood-waterlogging process (Fig. 12). Notably, the flood processes in the center of SC and NC are more susceptible to anthropogenic activities (Fig. 14), posing significant threats to lives and property.

5.3 Uncertainty and limitations

Although our study provided an estimation of the multi-dimensional characteristics of contiguous FCP events and first investigated their associated flood disasters and driving factors from an event-based perspective, there are several uncertainties and limitations that require further attention. It is essential to note that the 3D extreme rainfall features extracted with the different threshold values may have a different accumulated magnitude, projected area, lifespan, and moving distance. For instance, the accumulated areas of extreme rainfall extracted with the 95 % percentile of rainfall as a threshold may be smaller than that extracted with the 90 % percentile of rainfall. To accurately determine the appropriate extreme rainfall thresholds for multiple types of rainfall events needs to be further explored in further research. Meanwhile, the frequency of flood events cannot be accurately represented based on the current data resources in this study. Therefore, due to data limitations, only precipitation and flood features are considered in this study, and the temporal variations of frequency of flood were not analysed. Furthermore, flooding is a complex physical process that is typically influenced by a combination of natural and human factors. Though this paper only conducted a preliminary assessment of the relationships between flood disasters and driving factors, e.g., precipitation and flood features, environmental factors (cropland area, NDVI, slope, and difference elevation), and human activities factors (population and GDP), there may be other factors that probably exert important impact on flood disasters, such as hydraulic engineering projects (e.g., dams and reservoirs in mountain areas and flood-control measures in urban, as highlighted by Zhao et al. (2022) and Qi et al. (2022), which are very effective measures for mitigating the flood risk. Thus, it is necessary to integrate human activities and natural factors in further research to explore the mechanism of flood disasters. Overall, the 3D method can effectively capture the evolutionary patterns of contiguous FCP events. Strengthening research on extracting accurate precipitation characteristics and using more reasonable flood driving factors are expected to enhance our understanding of relationship between extreme precipitation and flood disasters in China.

6 Conclusions

Based on 1041 flood-causing precipitation events during the warm season (May to September) from 2000 to 2023 in China, this study developed an automatic precipitation event recognition algorithm using connected component 3D (CC3D) method. By employing this approach, we provided a detailed analysis of flood-causing precipitation (FCP) events and their triggered flood disasters from a 3D event-based perspective, and deeply investigated the complex relationship between flood disasters and precipitation, environment, and human activity factors. The research findings are summarized as follows.

A total 1041 flood disaster records were classified into 632 separate precipitation events, including 386 non-TC events and 246 TC events. It is found that TC-induced rainstorm events mostly occurred in the coastal areas of China, with the majority concentrated in coastal regions of Southern China (SC). These events are more inclined to move westward, and have a relatively small accumulated areas and magnitudes and short lifespans and moving distances. In contrast, the non-TC-induced FCP events are mainly clustered in SC and Northern China (NC). They tend to move eastward, with relatively larger accumulated magnitudes and affected areas, and have a longer lifespan and moving distance than TC events.

In contrast to the 3D features of extreme rainfall, flood characteristics, such as surface runoff and river discharge, show increasing trends, which are not statistically significant at the 0.05 level. At the same time, FCP events with high surface runoff are predominantly observed in the central SC and NC and northeastern NC. However, flood disasters, such as flood-affected population, direct economic losses, and affected cropland areas are more severe in the SC and parts of the NC than in the Northwestern China (NWC) and Qinghai-Tibetan Plateau (TP). Note that the number of deaths is relatively large in the NWC and the surrounding regions of TP, and significantly less in the center of SC, where there is a large affected population. Further analysis on the flood-affected ratio within the coverage areas of FCP events reveals that the spatial impact of floods on population and mortality exhibit significant spatial heterogeneity. In other words, the high flood affected population proportion is predominantly concentrated in SC, while high death rates are primarily distributed in the southeastern fringe of the TP and southwestern China. In terms of the ratio of direct economic losses, the small ratio events are mainly distributed in the southeastern SC, but relatively high events are in the western SC and northeastern NC. Regarding ratio of affected cropland, larger event can be found in the coastal areas of SC. Furthermore, our findings indicate that flood disasters represent a significant reduction in the past twenty years in China, except for the direct economic losses.

The results obtained by tracking the relationship between flood disaster and their driving factors reveal that precipitation features, especially accumulated magnitudes and lifespans of FCP events, are the most important driving factors, although precipitation factors and flood disasters exhibit distinct changing trends during 2000–2023. Meanwhile, the flood disasters events are significantly influenced by the human activities, but environmental factors have the lowest explanatory power. However, the interactive influence of any two factors is greater than that of the individual factors. Specifically, the interaction between precipitation factors and environmental factors displays significant nonlinear enhancement and bivariate enhancement effects. This means that although environmental factors have weak explanatory power on their own, the synergistic effects could exert the stronger influence due to their nonlinear characteristics at different spatial and temporal scales. It is worthwhile to note that the most flood disasters are mainly influenced by the combination of precipitation and environmental factors in China, whereas flood disasters events significantly influenced by the human activities are predominantly distributed in the center of SC and NC.

Code availability. The source code for our figures and identification of flood-causing precipitation events will be available upon request from the corresponding author.

Data availability. All observational and reanalysis data used in this work are publicly available. The historical flood disaster data from the Yearbook of Meteorological Disasters in China are available to download from https://navi.cnki.net/knavi/yearbooks/YQXZH/detail?uniplatform=NZKPT (last access: 19 August 2026). GloFAS-ERA5 river discharge reanalysis are accessible via https://doi.org/10.24381/cds.a4fdd6b9 (Joint Research Center, Copernicus Emergency Management Service, 2019). ERA5 surface runoff and precipitation datasets are accessible via the C3S Climate Data Store (https://cds.climate.copernicus.eu/datasets, last access: 10 May 2026). The NDVI, DEM, population and GDP dataset are derived from Resource and Environment Data Cloud Platform (http://www.resdc.cn, (last access: 19 August 2026)). The cropland datasets are obtained from https://doi.org/10.5281/zenodo.7936885 (Tu et al., 2023).

Author contributions. J.W.: Writing-original draft, Visualization, Methodology, Formal analysis, Data curation, Conceptualization, Funding acquisition. S.L.: Data curation, Software; X.G.: Funding acquisition, Writing-review, Supervision, Conceptualization. Y.H.: Supervision, Writing-review & editing. C.C.: Software. L.L.: Writing-review & editing. L.Z.: Writing-review & editing. A.K.P.: Writing-review & editing.

Competing interests. The contact author has declared that none of the authors has any competing interests.

Disclaimer. Publisher's note: Copernicus Publications remains neutral with regard to jurisdictional claims made in the text, published maps, institutional affiliations, or any other geographical representation in this paper. The authors bear the ultimate responsibility for providing appropriate place names. Views expressed in the text are those of the authors and do not necessarily reflect the views of the publisher.

Acknowledgements. We are grateful to the Editor Mihai Niculita and Ammar Abd Jasim and two anonymous referees for their careful evaluation of our manuscript. We also thank the Supercomputing Center of Lanzhou University for providing computational resources.

Financial support. This work was supported by the National Natural Science Foundation of China (42205193), the Open Foundation of Key Laboratory of Urban Meteorology (LUM-2025-14), the Funding for High-Level Talents in Lanzhou City (563225108), the Open Foundation of China Meteorological Administration Hydro-Meteorology Key Laboratory (23SWQXM001), the Ministry of Education's Humanities and Social Sciences Youth Fund (24YJCGJW008), and the Fundamental Research Funds for the Central Universities (lzujbky-2025-jdzx01).

Review statement. This paper was edited by Mihai Niculita and reviewed by Ammar Abd Jasim and two anonymous referees.

References

Allan, R. P., Willett, K. M., John, V. O., and Trent, T.: Global changes in water vapor 1979–2020, J. Geophys. Res.-Atmos. 127, e2022JD036728, https://doi.org/10.1029/2022JD036728, 2022.

Alpizar, M., Di Luca, A., Gachon, P., and Roberge, F.: Mesoscale Convective Systems in Northeastern North America: identification and evaluation with the convection-permitting version of the Canadian Regional Climate Model, Clim. Dynam., 64, 129, https://doi.org/10.1007/s00382-026-08102-6, 2026.

Asadieh, B. and Krakauer, N. Y.: Global trends in extreme precipitation: climate models versus observations, Hydrol. Earth Syst. Sci., 19, 877–891, https://doi.org/10.5194/hess-19-877-2015, 2015.

Ban, N., Schmidli, J., and Schär, C.: Heavy precipitation in a changing climate: Does short-term summer precipitation increase faster?, Geophys. Res. Lett., 42, 1165–1172, https://doi.org/10.1002/2014GL062588, 2015.

Blöschl, G., Hall, J., Viglione, A., Perdigão, R. A., Parajka, J., Merz, B., Lun, D., Arheimer, B., Aronica, G. T., and Bilibashi, A.: Changing climate both increases and decreases European river floods, Nature, 573, 108–111, https://doi.org/10.1038/s41586-019-1495-6, 2019.

Chan, S. C., Kendon, E. J., Fowler, H. J., Kahraman, A., Crook, J., Ban, N., and Prein, A. F.: Large-scale dynamics moderate impact-relevant changes to organised convective storms, Commun. Earth Environ., 4, https://doi.org/10.1038/s43247-022-00669-2, 2023.

Chen, X., Tian, S., Chen, N., Hu, G., Hou, R., and Peng, T.: Why did localized extreme rainfall trigger a rare mega flash flood in the mountains of western China?, Int. J. Disast. Risk Re., 116, 105090, https://doi.org/10.1016/j.ijdrr.2024.105090, 2025.

Chen, Y., Li, J., and Chen, A.: Does high risk mean high loss: Evidence from flood disaster in southern China, Sci. Total Environ., 785, 147127, https://doi.org/10.1016/j.scitotenv.2021.147127, 2021.

Chinita, M. J., Richardson, M., Teixeira, J., and Miranda, P. M.: Global mean frequency increases of daily and sub-daily heavy precipitation in ERA5, Environ. Res. Lett., 16, 074035, https://doi.org/10.1088/1748-9326/ac0caa, 2021.

Davenport, F. V., Burke, M., and Diffenbaugh, N. S.: Contribution of historical precipitation change to US flood damages, P. Natl. Acad. Sci. USA, 118, e2017524118, https://doi.org/10.1073/pnas.2017524118, 2021.

Deng, Y., Jiang, W., He, B., Chen, Z., and Jia, K.: Change in intensity and frequency of extreme precipitation and its possible teleconnection with large-scale climate index over the China from 1960 to 2015, J. Geophys. Res.-Atmos. 123, 2068–2081, https://doi.org/10.1002/2017JD027078, 2018.

Do, H. X., Westra, S., and Leonard, M.: A global-scale investigation of trends in annual maximum streamflow, J. Hydrol., 552, 28–43, https://doi.org/10.1016/j.jhydrol.2017.06.015, 2017.

Do, H. X., Mei, Y., and Gronewold, A. D.: To what extent are changes in flood magnitude related to changes in precipitation extremes?, Geophys. Res. Lett., 47, e2020GL088684, https://doi.org/10.1029/2020GL088684, 2020a.

Do, H. X., Zhao, F., Westra, S., Leonard, M., Gudmundsson, L., Boulange, J. E. S., Chang, J., Ciais, P., Gerten, D., Gosling, S. N., Müller Schmied, H., Stacke, T., Telteu, C.-E., and Wada, Y.: Historical and future changes in global flood magnitude – evidence from a model–observation investigation, Hydrol. Earth Syst. Sci., 24, 1543–1564, https://doi.org/10.5194/hess-24-1543-2020, 2020b.

Fang, Y., Du, S., Scussolini, P., Wen, J., He, C., Huang, Q., and Gao, J.: Rapid population growth in Chinese floodplains from 1990 to 2015, Int. J. Env. Res. Pub. He., 15, 1602, 2018.

Feng, J., Li, D., Li, Y., and Zhao, L.: Analysis of compound floods from storm surge and extreme precipitation in China, J. Hydrol., 627, 130402, https://doi.org/10.1016/j.jhydrol.2023.130402, 2023.

Feng, K., Wang, Y., Li, Y., Wang, F., Su, X., Zhang, Z., Wu, H., Zhang, G., Li, Y., and Wang, X.: Three-dimensional perspective on the characterization of the spatiotemporal propagation from meteorological to agricultural drought, Agr. Forest Meteorol., 353, 110048, https://doi.org/10.1016/j.agrformet.2024.110048, 2024.

Fowler, H. J., Lenderink, G., Prein, A. F., Westra, S., Allan, R. P., Ban, N., Barbero, R., Berg, P., Blenkinsop, S., Do, H. X., Guerreiro, S., Haerter, J. O., Kendon, E. J., Lewis, E., Schaer, C., Sharma, A., Villarini, G., Wasko, C., and Zhang, X.: Anthropogenic intensification of short-duration rainfall extremes, Nat. Rev. Earth Environ., 2, 107–122, https://doi.org/10.1038/s43017-020-00128-6, 2021.

Fu, G., Yu, J., Yu, X., Ouyang, R., Zhang, Y., Wang, P., Liu, W., and Min, L.: Temporal variation of extreme rainfall events in China, 1961–2009, J. Hydrol., 487, 48–59, https://doi.org/10.1016/j.jhydrol.2013.02.021, 2013.

Fu, S., Zhang, H., Zhong, Q., Chen, Q., Liu, A., Yang, J., and Pang, J.: Spatiotemporal variations of precipitation concentration influenced by large-scale climatic factors and potential links to flood-drought events across China 1958–2019, Atmos. Res., 282, 106507, https://doi.org/10.1016/j.atmosres.2022.106507, 2023.

Gu, X., Ye, L., Xin, Q., Zhang, C., Zeng, F., Nerantzaki, S. D., and Papalexiou, S. M.: Extreme precipitation in China: A review on statistical methods and applications, Adv. Water Resour., 163, 104144, https://doi.org/10.1016/j.advwatres.2022.104144, 2022.

Guan, X., Zang, Y., Meng, Y., Liu, Y., Lv, H., and Yan, D.: Study on spatiotemporal distribution characteristics of flood and drought disaster impacts on agriculture in China, Int. J. Disast. Risk Re., 64, 102504, https://doi.org/10.1016/j.ijdrr.2021.102504, 2021.

Harrigan, S., Zsoter, E., Alfieri, L., Prudhomme, C., Salamon, P., Wetterhall, F., Barnard, C., Cloke, H., and Pappenberger, F.: GloFAS-ERA5 operational global river discharge reanalysis 1979–present, Earth Syst. Sci. Data, 12, 2043–2060, https://doi.org/10.5194/essd-12-2043-2020, 2020.

Hersbach, H., Bell, B., Berrisford, P., Hirahara, S., Horányi, A., Muñoz-Sabater, J., and Thépaut, J. N.: The ERA5 global reanalysis, Q. J. Roy. Meteor. Soc., 146, 1999–2049, https://doi.org/10.1002/qj.3803, 2020.

Hiraga, Y., Watanabe, S., Yamashita, T., and Takizawa, H.: Climate change effects on probable maximum precipitation (PMP) of mesoscale convective systems: Model-based estimation and large ensemble-based frequency analysis, J. Hydrol., 661, 133724, https://doi.org/10.1016/j.jhydrol.2025.133724, 2025.

Hoang, D.-V. and Liou, Y.-A.: Assessing the influence of human activities on flash flood susceptibility in mountainous regions of Vietnam, Ecol. Indic., 158, 111417, https://doi.org/10.1016/j.ecolind.2023.111417, 2024.

Hodgkins, G. A., Whitfield, P. H., Burn, D. H., Hannaford, J., Renard, B., Stahl, K., Fleig, A. K., Madsen, H., Mediero, L., and Korhonen, J.: Climate-driven variability in the occurrence of major floods across North America and Europe, J. Hydrol., 552, 704–717, https://doi.org/10.1016/j.jhydrol.2017.07.027, 2017.

Islam, M. Z. and Wang, C.: Cost of high-level flooding as a consequence of climate change driver?: A case study of China's flood-prone regions, Ecol. Indic., 160, 111944, https://doi.org/10.1016/j.ecolind.2024.111944, 2024.

Jevrejeva, S., Jackson, L., Grinsted, A., Lincke, D., and Marzeion, B.: Flood damage costs under the sea level rise with warming of 1.5°C and 2°C, Environ. Res. Lett., 13, 074014, https://doi.org/10.1088/1748-9326/aacc76, 2018.

Jia, H., Chen, F., Pan, D., Du, E., Wang, L., Wang, N., and Yang, A.: Flood risk management in the Yangtze River basin–Comparison of 1998 and 2020 events, Int. J. Disast. Risk Re., 68, 102724, https://doi.org/10.1016/j.ijdrr.2021.102724, 2022.

Jiang, S. H., Wei, L. Y., Ren, L. L., Zhang, L. Q., Wang, M. H., and Cui, H.: Evaluation of IMERG, TMPA, ERA5, and CPC precipitation products over mainland China: Spatiotemporal patterns and extremes, Water Sci. Eng., 16, 45–56, https://doi.org/10.1016/j.wse.2022.05.001, 2023.

Joint Research Center, Copernicus Emergency Management Service: River discharge and related historical data from the Global Flood Awareness System, Early Warning Data Store (EWDS) [data set], https://doi.org/10.24381/cds.a4fdd6b9, 2019.

Ke, X., Wang, N., Xiu, Y., Dong, Z., and Wang, T.: A flash flood susceptibility prediction and partitioning method based on GeoDetector and random forest, Stoch. Env. Res. Risk A., 39, 1377–1404, https://doi.org/10.1007/s00477-025-02922-4, 2025.

Kharin, V. V., Zwiers, F. W., Zhang, X., and Wehner, M.: Changes in temperature and precipitation extremes in the CMIP5 ensemble, Clim. Change, 119, 345–357, https://doi.org/10.1007/s10584-013-0705-8, 2013.

Kundzewicz, Z. W., Kanae, S., Seneviratne, S. I., Handmer, J., Nicholls, N., Peduzzi, P., Mechler, R., Bouwer, L. M., Arnell, N., and Mach, K.: Flood risk and climate change: global and regional perspectives, Hydrol. Sci. J., 59, 1–28, https://doi.org/10.1080/02626667.2013.857411, 2014.

Li, K., Wu, S., Dai, E., and Xu, Z.: Flood loss analysis and quantitative risk assessment in China, Nat. Hazards, 63, 737–760, https://doi.org/10.1007/s11069-012-0180-y, 2012.

Li, Y. and Zhao, D.: Climatology of tropical cyclone extreme rainfall over China from 1960 to 2019, Adv. Atmos. Sci., 39, 320–332, https://doi.org/10.1007/s00376-021-1080-4, 2022.

Lim, W. H., Yamazaki, D., Koirala, S., Hirabayashi, Y., Kanae, S., Dadson, S. J., Hall, J. W., and Sun, F.: Long-term changes in global socioeconomic benefits of flood defences and residual risk based on CMIP5 climate models, Earth's Future, 6, 938–954, https://doi.org/10.1002/2017EF000671, 2018.

Liu, Y., Yang, Z., Huang, Y., and Liu, C.: Spatiotemporal evolution and driving factors of China's flash flood disasters since 1949, Sci. China Earth Sci., 61, 1804–1817, https://doi.org/10.1007/s11430-017-9238-7, 2018.

Lu, W., Lei, H., Yang, W., Yang, J., and Yang, D.: Comparison of floods driven by tropical cyclones and monsoons in the southeastern coastal region of China, J. Hydrometeorol., 21, 1589–1603, https://doi.org/10.1175/JHM-D-20-0002.1, 2020.

Ma, S., Zhou, T., Dai, A., and Han, Z.: Observed changes in the distributions of daily precipitation frequency and amount over China from 1960 to 2013, J. Climate, 28, 6960–6978, https://doi.org/10.1175/JCLI-D-15-0011.1, 2015.

Mallakpour, I. and Villarini, G.: The changing nature of flooding across the central United States, Nat. Clim. Change, 5, 250–254, https://doi.org/10.1038/nclimate2516, 2015.

Qi, W., Ma, C., Xu, H., and Zhao, K.: Urban flood response analysis for designed rainstorms with different characteristics based on a tracer-aided modeling simulation, J. Clean. Prod., 355, 131797, https://doi.org/10.1016/j.jclepro.2022.131797, 2022.

Rashid, M., Wahl, T., Villarini, G., and Sharma, A.: Fluvial flood losses in the contiguous United States under climate change, Earth's Future, 11, e2022EF003328, https://doi.org/10.1029/2022EF003328, 2023.

Rentschler, J., Salhab, M., and Jafino, B. A.: Flood exposure and poverty in 188 countries, Nat. Commun., 13, 3527, https://doi.org/10.1038/s41467-022-30727-4, 2022.

Rogers, J., Maneta, M., Sain, S., Madaus, L., and Hacker, J.: The role of climate and population change in global flood exposure and vulnerability, Nat. Commun., 16, 1287, https://doi.org/10.1038/s41467-025-56654-8, 2025.

Sharma, A., Wasko, C., and Lettenmaier, D. P.: If precipitation extremes are increasing, why aren't floods?, Water Resour. Res., 54, 8545–8551, https://doi.org/10.1029/2018WR023749, 2018.

Shi, J., Cui, L., and Tian, Z.: Spatial and temporal distribution and trend in flood and drought disasters in East China, Environ. Res., 185, 109406, https://doi.org/10.1016/j.envres.2020.109406, 2020.

Silversmith, W.: cc3d: Connected components on multilabel 3D & 2D images, Zenodo, https://doi.org/10.5281/zenodo.5719536, 2021.

Tang, R., Dai, Z., Mei, X., and Lou, Y.: Joint impacts of dams and floodplain on the rainfall-induced extreme flood in the Changjiang (Yangtze) River, J. Hydrol., 627, 130428, https://doi.org/10.1016/j.jhydrol.2023.130428, 2023.

Teale, N. and Winter, J. M.: The Relationship between Extreme Precipitation and Damaging Floods in the Northeastern United States, J. Appl. Meteorol. Clim., 63, 1035–1047, https://doi.org/10.1175/JAMC-D-23-0156.1, 2024.

Thackeray, C. W., Hall, A., Norris, J., and Chen, D.: Constraining the increased frequency of global precipitation extremes under warming, Nat. Clim. Change, 12, 441–448, https://doi.org/10.1038/s41558-022-01329-1, 2022.

Trenberth, K. E., Dai, A., Rasmussen, R. M., and Parsons, D. B.: The changing character of precipitation, B. Am. Meteor. Soc., 84, 1205–1218, https://doi.org/10.1175/BAMS-84-9-1205, 2003.

Tu, Y., Wu, S., Chen, B., Weng, Q., Bai, Y., Yang, J., Yu, L., and Xu, B.: A 30 m annual cropland dataset of China from 1986 to 2021 (Version v0), Zenodo [data set], https://doi.org/10.5281/zenodo.7936885, 2023.

Tu, Y., Wu, S., Chen, B., Weng, Q., Bai, Y., Yang, J., Yu, L., and Xu, B.: A 30 m annual cropland dataset of China from 1986 to 2021, Earth Syst. Sci. Data, 16, 2297–2316, https://doi.org/10.5194/essd-16-2297-2024, 2024.

Wang, J. and Hu, Y.: Environmental health risk detection with GeogDetector, Environ. Modell. Softw., 33, 114–115, https://doi.org/10.1016/j.envsoft.2012.01.015, 2012.

Wang, J., Li, X. H., Christakos, G., Liao, Y. L., Zhang, T., Gu, X., and Zheng, X. Y.: Geographical detectors-based health risk assessment and its application in the neural tube defects study of the Heshun Region, China, Int. J. Geogr. Inf. Sci., 24, 107–127, https://doi.org/10.1080/13658810802443457, 2010.

Wang, J., Guan, X., and Miao, S.: Spatiotemporal evolution patterns of flood-causing rainstorm events in China from a 3D perspective, Atmos. Res., 315, 107920, https://doi.org/10.1016/j.atmosres.2025.107920, 2025.

Wang, X., Luo, M., Wu, S., Ning, G., Liu, Z., Wang, S., Wang, P., Zhang, H., and Li, X.: Spatiotemporal evolution patterns of contiguous extreme precipitation events across China from a 3D perspective, Geophys. Res. Lett., 49, e2022GL098840, https://doi.org/10.1029/2022GL098840, 2022a.

Wang, Y., Li, C., Liu, M., Cui, Q., Wang, H., Lv, J., Li, B., Xiong, Z., and Hu, Y.: Spatial characteristics and driving factors of urban flooding in Chinese megacities, J. Hydrol., 613, 128464, https://doi.org/10.1016/j.jhydrol.2022.128464, 2022b.

Wasko, C., Nathan, R., Stein, L., and O'Shea, D.: Evidence of shorter more extreme rainfalls and increased flood variability under climate change, J. Hydrol., 603, 126994, https://doi.org/10.1016/j.jhydrol.2021.126994, 2021.

Wasko, C., Westra, S., Nathan, R., Pepler, A., Raupach, T. H., Dowdy, A., Johnson, F., Ho, M., McInnes, K. L., Jakob, D., Evans, J., Villarini, G., and Fowler, H. J.: A systematic review of climate change science relevant to Australian design flood estimation, Hydrol. Earth Syst. Sci., 28, 1251–1285, https://doi.org/10.5194/hess-28-1251-2024, 2024.

Wei, L., Hu, K., and Hu, X.: Rainfall occurrence and its relation to flood damage in China from 2000 to 2015, J. Mt. Sci. 15, 2492–2504, https://doi.org/10.1007/s11629-018-4931-4, 2018.

Westra, S., Alexander, L. V., and Zwiers, F. W.: Global increasing trends in annual maximum daily precipitation, J. Climate, 26, 3904–3918, https://doi.org/10.1175/JCLI-D-12-00502.1, 2013.

Wu, J., Han, G., Zhou, H., and Li, N.: Economic development and declining vulnerability to climate-related disasters in China, Environ. Res. Lett., 13, 034013, https://doi.org/10.1088/1748-9326/aaabd7, 2018.

Wu, M., Wu, Z., Ge, W., Wang, H., Shen, Y., and Jiang, M.: Identification of sensitivity indicators of urban rainstorm flood disasters: A case study in China, J. Hydrol., 599, 126393, https://doi.org/10.1016/j.jhydrol.2021.126393, 2021.

Wu, Y., Ji, H., Wen, J., Wu, S.-Y., Xu, M., Tagle, F., He, B., Duan, W., and Li, J.: The characteristics of regional heavy precipitation events over eastern monsoon China during 1960–2013, Global Planet. Change, 172, 414–427, https://doi.org/10.1016/j.gloplacha.2018.11.001, 2019.

Xie, Z., Du, Y., Zeng, Y., and Miao, Q.: Classification of yearly extreme precipitation events and associated flood risk in the Yangtze-Huaihe River Valley, Sci. China Earth Sci., 61, 1341–1356, https://doi.org/10.1007/s11430-017-9212-8, 2018.

Zhang, H. and Zhai, P.: Temporal and spatial characteristics of extreme hourly precipitation over eastern China in the warm season, Adv. Atmos. Sci., 28, 1177–1183, https://doi.org/10.1007/s00376-011-0020-0, 2011.

Zhang, W., Leung, Y., and Wang, Y.: Cluster analysis of post-landfall tracks of landfalling tropical cyclones over China, Clim. Dynam., 40, 1237–1255, https://doi.org/10.1007/s00382-012-1519-5, 2013.

Zhao, M., Liu, Y., Wang, Y., Chen, Y., and Ding, W.: Effectiveness assessment of reservoir projects for flash flood control, water supply and irrigation in Wangmo Basin, China, Sci. Total Environ. 851, 157918, https://doi.org/10.1016/j.scitotenv.2022.157918, 2022.